energies

MDPI

Article

Evaluation of Integrated Concepts with CO_2 for Heating, Cooling and Hot Water Production

Silje Smitt [1,*], Ángel Pardiñas [2] and Armin Hafner [1]

[1] Department of Energy and Process Engineering, Norwegian University of Science and Technology, Kolbjørn Hejes vei 1D, 7491 Trondheim, Norway; armin.hafner@ntnu.no
[2] SINTEF Energy Research, Kolbjørn Hejes vei 1D, 7465 Trondheim, Norway; angel.a.pardinas@sintef.no
* Correspondence: silje.smitt@ntnu.no

Abstract: The hotel sector is characterized by high thermal demands and a large carbon footprint, which greatly contributes to the global warming effect. Consequently, there is a need to investigate solutions that can reduce energy usage within this sector by means of environmentally friendly and sustainable technologies. Integrated CO_2 heat pump systems for heating, cooling, and hot water production in hotels have demonstrated promising results. This paper theoretically compares the energy consumption, environmental impact, and cost of three different design concepts for integrated CO_2 units equipped with thermal storage. The main characteristics of the evaluated designs are single-stage compression, parallel compression, and ejector-supported parallel compression. Furthermore, two separate hot water charging strategies were implemented and investigated over a large span of ambient temperatures and loads. The evaluations were carried out by considering eight different European locations, ranging from Scandinavia to the Mediterranean. The results revealed that the ejector-supported parallel compression design was superior in terms of annual COP, which was found to be in the range of 4.27 to 5.01 for the Scandinavian locations and 5.03 to 5.71 for the other European locations. When accounting for investment cost and electricity prices, the payback period at the Scandinavian locations was 6.3 to 7.7 years. Payback periods of 3 and 4.5 to 7.5 were obtained for hotels located in the temperate and Mediterranean climates, respectively. The investigation also revealed that the hot water charging strategy, rather than the specific CO_2 heat pump design, is the least expensive measure to enhance performance.

Keywords: heat pump; system design; heating and cooling; hotels; CO_2; thermal storage; numerical modeling; concept evaluation

Citation: Smitt, S.; Pardiñas, Á.; Hafner, A. Evaluation of Integrated Concepts with CO_2 for Heating, Cooling and Hot Water Production. *Energies* **2021**, *14*, 4103. https://doi.org/10.3390/en14144103

Academic Editor: Dimitris Katsaprakakis

Received: 11 June 2021
Accepted: 30 June 2021
Published: 7 July 2021

1. Introduction

Different actors are involved in a global and intersectoral effort to achieve the 2-degree goal of the Paris Agreement by limiting CO_2 emissions through efficiency and reduction of energy demands [1]. Energy use in buildings involves approximately 18% of greenhouse gas emissions globally. A staggering one-third of these emissions are linked to commercial buildings, such as hotels [2]. Similar numbers are given for Europe, with the commercial sector being responsible for one-third of the total energy consumption and related emissions in buildings [3]. Thus, measures to increase efficiency by improved technology, management, and integration of demands in the hotel sector will significantly contribute towards realizing the goals of the Paris Agreement. Estimations indicate a potential in energy saving within the commercial sector of approximately 30% [4,5]. This is particularly important as the tourism sector is estimated to increase by 3.8% annually until 2030 [6].

The dominant thermal demands in hotels include domestic hot water (DHW) production, space heating (SH), and cooling, with the share between them depending on hotel location or quality of construction (level of insulation), among other factors. For SH and

DHW, Nordic hotels have been utilizing conventional thermal energy sources, e.g., electric boilers with inefficient central systems [7], justified by relatively low electricity prices. Within Europe in general, fossil fuel-fired boilers still represent the most applied heating source [5]. In the past decade, district heating and cooling networks have gained solid footing and are becoming important in Scandinavia [8,9]. Yet, separate chillers, i.e., vapor compression units, are generally utilized to fulfill the cooling demands in hotels, even if access to the district cooling network exists at the location. Heat pumps appear as a suitable alternative to meet all the different demands with a single unit while boosting energy efficiency and reducing operational costs. This is achieved through their principle of operation of upgrading heat from one temperature level to another with a considerably low input of work, namely, electricity. Furthermore, a recent five-year study of hotels in Nordic countries has shown that the specific energy consumption in hotels with heat pumps as the primary heat source is lowest compared to those using alternative systems, such as electric boilers or district heating [10].

Heat pumps are vapor compression systems that transfer heat from a heat source at relatively low temperature, e.g., air, water, ground, or chilling water loop, to a heat sink at a higher temperature, such as a SH circuit or hot water tanks. Heat is transferred through a fluid, i.e., refrigerant, which is circulated and adapted to the required temperature levels by means of work input to a compressor. Refrigerant selection has been a hot topic in the last decades, mainly as the historically favored synthetic refrigerants are, or have been, responsible for significant environmental consequences, either destruction of the ozone layer by CFCs (chlorofluorocarbons) and HCFCs (hydrochlorofluorocarbons) or global warming by HFCs (hydrofluorocrbons). Natural refrigerants, such as ammonia, CO_2, and hydrocarbons, are widely utilized in different applications and have the potential to replace synthetic refrigerants in heat pumps and chillers. The natural refrigerants were among the first utilized in vapor compression systems and have negligible impact on the environment, but can introduce challenges in terms of toxicity, operation at high pressure, or flammability [11]. Natural refrigerants are competing for the niche of heat pumps with the newly developed HFOs (hydrofluoroolefins), which fulfill the requirements of low global warming potential (GWP) dictated by several national or international regulations, e.g., F-gas in Europe. However, recent studies and reports have raised concerns regarding the HFO's decomposition product trifluoroacetic acid (TFA). Widespread and long-term application of HFOs can result in TFA accumulating in drinking water, which can have severe effects on human health and the environment [12]. In addition, a newly published report demonstrates that one of the most applied HFOs (HFO-1234ze) in current use ultimately decomposes partially into the refrigerant R23; one of the most potent greenhouse gases known (100-year GWP of 14,800) [13]. Although a recent study predicts that HFOs, HFCs and their mixtures will still have a significant market share as far as 2030 [14], it could be agreed that natural refrigerants are the long-term solution, and among them CO_2 (GWP = 1) appears as a safe and sustainable choice for commercial heat pumps, e.g., for hotels. CO_2 has had a success story in commercial refrigeration (centralized units, condensing units, and plugins). Now, CO_2 is becoming a competing alternative in other sectors, such as industrial refrigeration, due to factors like increased efficiency and component size, reductions in operational costs (economy of scale), and legislation [15].

Due to its low critical temperature (31 °C), CO_2 applications were initially limited to operations where heat rejection (condenser) would happen well below the critical point, such as freezing in cascade refrigeration units. The implementation of CO_2 in heat pumps and commercial refrigeration, which can operate with heat rejection or production above CO_2's critical temperature, was realized thanks to the investigations of Gustav Lorentzen and his team. Lorentzen (1994) [16] presented the basic layout of a transcritical CO_2 heat pump, based on a system with suction accumulator, high-pressure control through the valve feeding the evaporator, and the application of a gas cooler in place of the condenser. At the time, this unit was suggested as an efficient and environmentally friendly replacement of R12 in mobile air conditioning (AC) [17]. Nekså et al. (1998) [18] stated that transcritical

CO_2 heat pumps are suitable to produce DHW, as the temperature glide in the refrigerant side of the gas cooler follows nearly perfectly the relatively large temperature difference in the waterside, reaching up to 90 °C. Additionally, Nekså (2002) [19] mentioned other applications for CO_2 heat pumps that, with the course of years, were realized, e.g., SH and residential heat pumps and heat pump dryers. Stene (2005) [20] investigated the efficient integration of SH and DHW to maximize the use of the gliding heat rejection of CO_2 heat pumps. The concept is based on splitting the gas cooler into three parts connected in series: the warmest and coldest parts to reheat and preheat DHW, and the intermediate part to produce SH. Thus, it is possible to minimize CO_2 temperature downstream of the gas cooler, reducing expansion losses and improving the performance. Tosato et al. (2020) [21] performed an experimental and numerical investigation of a newly developed CO_2 air/water reversible heat pump, intended for household applications. The system was evaluated at a range of ambient temperatures (−2.0 to 11.2 °C), and at DHW setpoint temperatures ranging from 60 to 80 °C. The results illustrated that the highest COP was achieved at DHW setpoint temperature of 60 °C, due to an increase in DHW mass flow rate through the gas cooler. However, charging time was significantly reduced in comparison to when setpoints of 70 and 80 °C were applied. Dai et al. (2019) [22] suggested using mechanical subcooling in CO_2 transcritical heat pump cycle to reduce the gas cooler outlet temperature. They found that the primary energy consumption was reduced compared to a conventional transcritical single-stage CO_2 heat pump, which resulted in additional reductions in emissions of around 16%. Emissions were reduced by approximately 18–33% and 62–69% compared to a coal-fired boiler and direct electric heating, respectively.

Another measure to increase the system efficiency of CO_2 heat pumps is simultaneous production of DHW and cooling. Byrne et al. (2009) [23] investigated a CO_2 heat pump layout for simultaneous production of heating and cooling aimed at hotels, luxury dwellings, or smaller office buildings. The system design is based on a division of the gas cooler into three parts: a DHW heat exchanger, a SH heat exchanger, and a subcooler that heats water to defrost a backup air evaporator. This air evaporator is necessary to balance the system when the space cooling demand is an insufficient heat source to achieve the heating demand. The authors performed a numerical study to compare this heat pump architecture operating with CO_2 and with R407C, and observed that CO_2 can outperform the HFC in terms of environmental impact. Diaby et al. (2019) [24] is a continuation of the previous work, as the authors present heat pump models for either simultaneous cooling, SH, and DHW or desalination. The numerical results in both cases are satisfactory, and the authors conclude that CO_2 is an exceptionally suited refrigerant for multipurpose heat pumps compared to "standard" refrigerants. This statement is supported by the conclusions in the study from Liu et al. (2016) [25], where the purpose of the heat pumps would be cooling and heating processes in food processing industries. An experimental study of combined AC and DHW production with a CO_2 heat pump is introduced in Adriansyah (2004) [26]. The results revealed a combined (heating and cooling) coefficient of performance (COP) as high as 8 when all the heat available in the gas cooler can be recovered. Farsi et al. (2016) [27] delved into the use of heat pumps for combined cooling and desalination, and the authors indicate the potential of CO_2 to improve desalination. Moreover, energy savings are maximized and the total annual cost is reduced when compared to separate systems (CO_2 refrigeration system and a desalination unit using steam from a boiler run with methane). Singh et al. (2020) [28] presented numerical simulations of a planned installations of a 140 kW transcritical CO_2 heat pump for a centralized kitchen in Bangalore, India. The heat pump will preheat hot water to 90 °C for steam production while supplying AC cooling for the entire building and utilizing thermal storage to compensate for asynchronous thermal demands. Simulations illustrated that the system can achieve a COP above 6 when operating in combined heating and cooling mode. The total energy consumption is expected to be reduced by 33% compared to the current solution, which will reduce yearly $CO_{2\text{-eq}}$ emissions by about 300 tonnes.

CO_2 heat pumps are increasing their presence in the portfolio of different manufacturers in Europe, in some cases adapting existing compressor packs for commercial refrigeration. An example of this is shown in Smitt et al. (2020) [29], with a performance analysis based on field measurements of a CO_2 heat pump for integrated production of heating and cooling with a 6 m^3 thermal storage. The study evaluates how different demands change during the specific year and how they affect the different performance indicators. One of the main conclusions of this study is that COPs improve with DHW charging (compared to SH only), meaning that DHW charging strategy is crucial to boost efficiency. A later numerical study of the same system demonstrated how the energy savings could be reduced with 5.8–13.2% for different seasonal scenarios when charging the DHW storage at low loads [30]. Additional perks of applying the low load charging strategy were reduced peak power usage, operational fluctuations, and ON/OFF cycles.

A dedicated and more complex CO_2 heat pump architecture is introduced in Tosato et al. (2020) [31], including two-stage evaporation supported by ejector (heat source or AC production, depending on operation mode). Results from a limited period in winter are presented, indicating a good efficiency with DHW production and the benefit of developing control strategies to minimize start and stops. The potential of evaporation in two stages was not fully evaluated with the available data in Tosato et al. (2020) [31]. The first results in summer mode for the aforementioned CO_2 heat pump were presented in Hafner et al. (2020) [32], showing COPs around 5 when producing chilled water at 7 °C (from 11 °C) and DHW at 60 °C (from 30 °C). The authors concluded that the potential of two-stage evaporation with an ejector could not be fully utilized unless higher waterside temperature differences are allowed in the evaporators.

In contrast to most of the previous articles and references, which analyzed or introduced rather simple layouts for CO_2 heat pumps, this work presents sophisticated architectures applicable for hotels, which are evaluated numerically with transient models. These systems include ejectors, parallel compression, and combined air-to-CO_2 evaporators/gas coolers, which can be applied as either heat source or sink. Load profiles are established based on previous analysis of a medium-sized hotel, and the performance is determined for each heat pump architecture and according to the climate of different cities in Scandinavia. Additional locations in Central Europe and the Mediterranean are included to evaluate the feasibility of such installations in warmer climates. Two separate DHW charging strategies are implemented to evaluate the influence of charging strategy in comparison to design with respect to performance. The sustainability of each design is investigated in terms of annual global warming contribution at each location. An economic evaluation is included to discuss whether these CO_2 heat pumps are cost-efficient compared to more conventional approaches, including electric boilers and separate chillers for AC cooling applications.

2. System Description

The approach of the integrated solution with CO_2 is to use a single unit with a flexible design to supply SH, DHW, and AC within the building. The simplified schematic of an integrated CO_2 unit with a standard single-stage compression (SC) is shown in Figure 1. The main system components are four compressors, a gas cooler section for heat production, AC evaporators, an intermediate temperature (INT) liquid receiver, and four air evaporators that can be employed as gas coolers for heat rejection when surplus heat is produced. The integrated unit is dimensioned to operate in the Scandinavian ambient-temperature range, from −15 to 35 °C. In addition to SC integrated system design, which is described in Section 2.1, two alternative system configurations are presented in Section 2.2 to investigate measures that can enhance efficiency. Note that ambient air has been selected as the main heat source for all configurations. Superior heat sources, such as seawater and boreholes, could be applied in place of ambient air. However, alternative heat sources are highly dependent on the building's specific location and would not be applicable everywhere. As a result, air heat exchangers are applied in all system configurations.

2.1. Design and Operation

Figure 1 illustrates the SC integrated CO_2 unit. The evaporation level consists of four ambient air fin-and-tube evaporators and two glycol AC heat exchangers, which function to supply the heating and cooling load, respectively. Simultaneous operation with both air and glycol evaporators is limited, as SH and AC cooling loads are rarely concurrent. The cooling demand of the building is realized by employing the plate evaporators, $EVAP_{AC,1}$ and $EVAP_{AC,2}$ in Figure 1, which supply chilled glycol to the AC units in the building. Each evaporator's thermostatic expansion valve controls the mass flow of CO_2 according to the superheat at the exit of the respective unit. The mass flow of glycol is controlled to achieve the AC setpoint temperature.

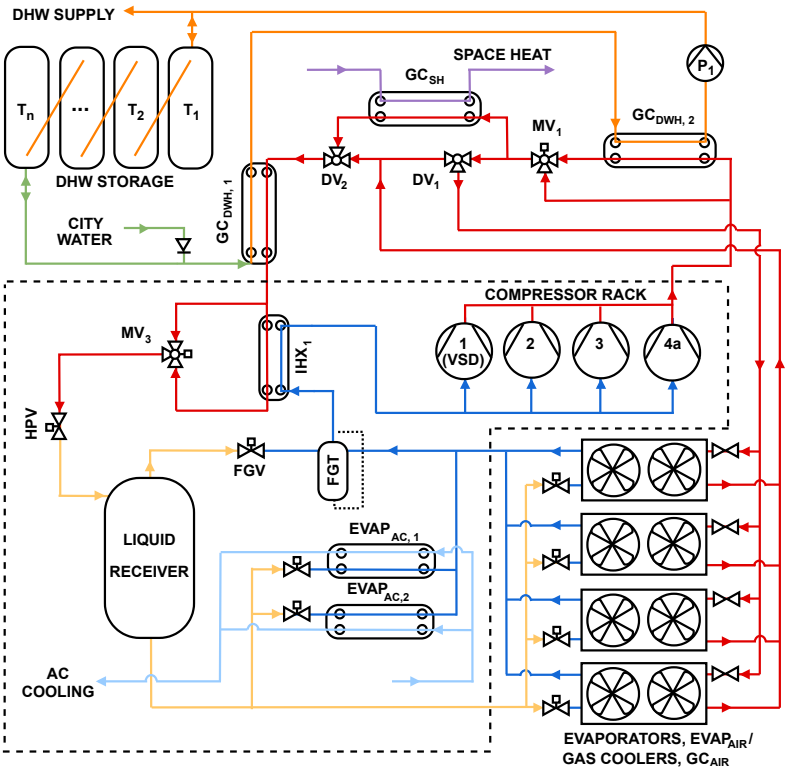

Figure 1. Simplified representation of the standard integrated CO_2 concept, equipped with single-stage compression (SC). High-pressure lines are indicated in red, intermediate pressure lines in yellow, and low-pressure lines in dark blue.

The fin-and-tube heat exchangers are exclusively connected to either the high-pressure side (red line) for gas coolers operation or the low-pressure line (dark blue) for evaporation at low temperature (LT). The distribution lines through the heat exchangers are switched between the different pressure levels, dependent on the mode of operation. Traditionally, a design selection with separate evaporators and gas coolers is preferred for simplicity and heat transfer considerations. However, due to advances within heat exchanger development and operation, several suppliers offer combined units to reduce the investment cost. The air heat exchangers are employed according to the heating demand of the building when operating in evaporator mode. Airflow through the evaporators is controlled by fans equipped with high-efficiency brushless DC motors. The CO_2 evaporation pressure is controlled by the thermostatic expansion valves, which secure a superheat at the exit of each evaporation unit. The superheat is fixed to a minimum, such that enhanced heat transfer is achieved in the heat exchangers. The suction accumulator and the internal heat exchanger, FGT and IHX_1 in Figure 1, respectively, ensure no liquid carryover to the compressors.

The CO_2 compressors remove vapor from the evaporator pressure level and discharge it to the gas coolers at high pressure. The compressor rack consists of four parallel piston compressors, in which compressor 1 in Figure 1 is equipped with a variable speed drive (VSD). Compressors 2 to 4 operate at a fixed speed and are controlled by ON/OFF, while the VSD compressor continuously adjusts the compressor section capacity according to demand. Thus, a broad range of capacities can be achieved by employing the VSD compressor alongside various combinations of the fixed compressors. The number of active compressors is determined based on the magnitude and combination of thermal demands; typically, high SH and DHW demands at low ambient temperatures and high AC cooling demands at high ambient temperatures.

The CO_2 gas cooler section is applied for heat recovery to SH and DHW, heat rejection to the ambient, or as a combination of the aforementioned. When heat rejection to the ambient is required, the directional valve, DV_1, directs the flow towards the air-cooled gas coolers, GC_{air}. The gas cooler section producing SH, GC_{SH}, are in these instances bypassed. The number of gas cooler units employed is determined based on the AC cooling and the DHW demand.

The main CO_2 gas cooler section consists of three plate heat exchangers that supply heat for DHW and SH. The temperature span of each heat exchanger is arranged according to the transcritical temperature glide of CO_2 [20]. Preheating of the DHW takes place at the lower end of the CO_2 temperature glide, in $GC_{DHW,1}$, as cold city water enters the heat exchanger. The DHW is further reheated to its setpoint temperature in $GC_{DHW,2}$. The modulating valve, MV_1, continuously controls the flow of CO_2 through $GC_{DHW,2}$ to reach the DHW setpoint temperature. Thus, the load distribution between $GC_{DHW,1}$ and $GC_{DHW,2}$ automatically adjust according to the load and temperature profile of the mid heat exchanger, GC_{SH}. For instance, the majority of the DHW load is rejected through $GC_{DHW,1}$ when the SH demand and setpoint temperature are high. During operations with low SH demand, most of the DHW load is rejected through $GC_{DHW,2}$. This configuration enables continuous low load production of DHW, which in turn reduces gas cooler outlet temperature and enhances overall system COP [30]. The requested DHW heating load is determined based on the energy reserve in the DHW storage, constituted by the temperature and volume in the storage tanks.

The storage, which is shown in Figure 1, has a water volume of 6 m^3 and is comprised of hot water tanks connected in series. The energy reserve is calculated based on the temperature boundary across the storage. At times when the temperature in the storage is low, a signal is sent to the DHW pump, P_1, to increase the mass flow and thus DHW charging load. DHW enters the first tank in the series, T_1, and the hot water boundary gradually moves across the storage from right to left during charging. Cold water is supplied from city water or drawn from the last tank, T_n, and is directed towards preheating. The storage is fully charged when the last tank in the series, T_n, reaches a high and uniform temperature.

The control of the high pressure is achieved with the high-pressure valve (HPV) in Figure 1. The integrated unit typically operates in the transcritical region (above 73.8 bar) to ensure the DHW setpoint temperature is reached. The maximum operating pressure of the system is 105 bar. After expansion, liquid enters the receiver, which holds a pressure between 36 to 50 bar. The receiver pressure is controlled by the flash gas valve, FGV, and is regulated according to evaporating pressure. During operations with low ambient temperature and high heating loads, receiver pressure is reduced to limit the vapor fraction at the inlet of the evaporators.

2.2. Alternative System Configurations

Two alternative system designs are presented in Figure 2. Both configurations, (a) parallel compression (PC) and (b) ejector-supported parallel compression (EJ), introduce compression from the liquid receiver at INT pressure level. Compressors 2 and 3 are equipped with pivoting suction ports, which directions are controlled by DV_3 and DV_4,

respectively. The pivoting suction port of the particular compressor refers to the possibility of selecting the suction manifold connection and integrating it in either the LT section or the INT parallel section. Thus, flexibility is significantly enhanced as the integrated system can swiftly adapt the number of compressors assigned to a particular suction group [33]. Both pivoting compressors work in support of the LT base compressor at low ambient temperature and high SH loads. During operational conditions with high ambient temperatures and dominant AC cooling loads, the pivoting compressors are employed at the INT level. Thus, the number of compressors employed at each pressure level is adjusted to meet both heating and cooling loads without the need for additional compressors.

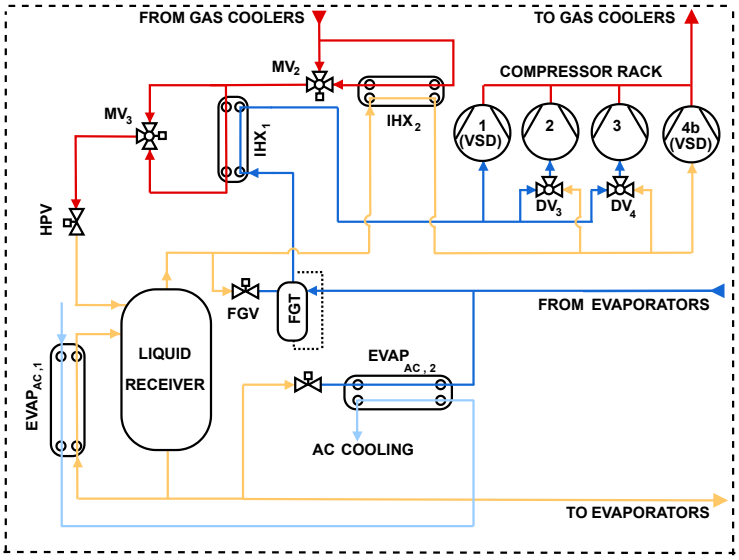

a) Parallel compression (PC)

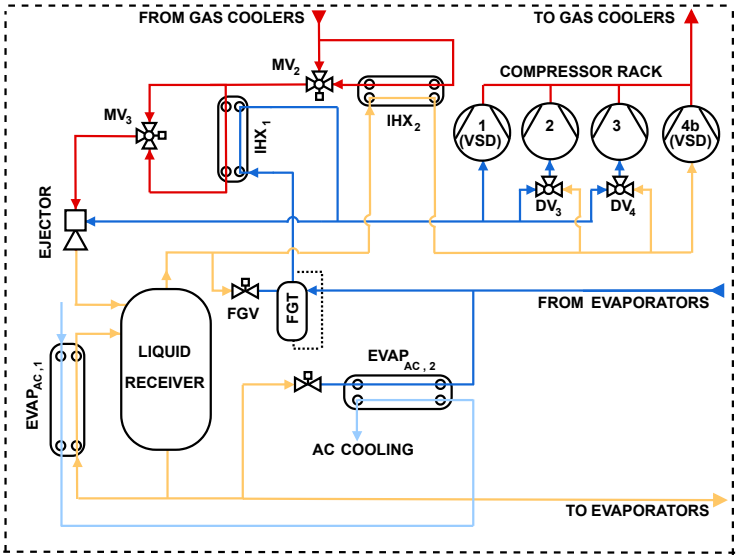

b) Ejector-supported parallel compression (EJ)

Figure 2. Alternative design of CO_2 integrated system with (**a**) parallel compression (PC), and (**b**) ejector-supported parallel compression (EJ).

Both configurations presented in Figure 2 are equipped with two AC evaporators, which are applied to provide cooling in series at different pressure levels. $EVAP_{AC,1}$ is installed at the INT pressure level and relies on gravity self-circulation from the liquid receiver. The evaporator is installed below the liquid receiver and is fed through a liquid column from the bottom of the receiver, creating a static pressure difference. The cooling load is determined based on the chilled water mass flow rate and the INT pressure level.

The parallel compressor section controls the latter in order to meet the total cooling demand from the building. $EVAP_{AC,2}$ is installed at the LT evaporation level and ensures cooling of the chilled water to setpoint conditions.

The HPV in Figure 2a is replaced by a ejector block in Figure 2b. The ejector is connected to the high-pressure side and recovers the expansion work in the high-pressure stream to lift the pressure of refrigerant from the LT pressure level. The vapor ejector operates in parallel to the LT compressors and is installed downstream of IHX_1, and so provides a dual benefit. First, it ensures a high value of superheat at the suction port of both the ejector and the compressor, which allows the evaporators to operate with a low superheat. Second, additional cooling downstream of the gas cooler is provided to reduce expansion losses. Typically, applications of ejectors demonstrate the largest benefits when the gas cooler outlet temperature is elevated. Such a scenario transpires in both winter and summer when either SH or AC cooling loads are high and DHW demands are low.

2.3. Operational Modes

The system designs have been established to provide flexibility and a high degree of operational freedom independent of the specific mode of operation, e.g., summer and winter.

2.3.1. Winter Mode

The air evaporators shown in Figure 1, $EVAP_{air}$, are employed based on SH demand. Vapor is sucked from $EVAP_{air}$ through IHX_1 by the LT base compressors. The compressor capacity is mainly controlled by the SH demand, as additional heat for DHW is continuously recovered as a byproduct if needed. Neither of the AC cooling evaporators is active during winter mode. For the the system solutions shown in Figure 2, parallel compressors are employed to remove flash gas from the system and control the pressure of the liquid receiver. The number of compressors employed at LT and INT pressure levels is determined based on heating demand. Vapor from the liquid receiver is superheated in IHX_2 before compression. The ejector in Figure 2b introduces expansion work recovery from the high pressure level. Thus, a portion of the required compressor capacity is moved from the LT section to the INT section, reducing the total work of the system.

2.3.2. Summer Mode

The base compressor capacity is controlled by the cooling load, as the LT pressure is regulated to meet the requested AC cooling demand of the building. The mass flow rate of chilled water is controlled to meet the setpoint at the outlet of the AC evaporators. For the AC-chiller arrangements presented in Figure 2, two separate pressure levels are used to chill down the liquid. After the first stage of cooling, chilled water from $EVAP_{AC,1}$ is directed to the second AC evaporator, $EVAP_{AC,2}$, for further cooling until the setpoint is reached. $EVAP_{AC,2}$ is installed in parallel to the air evaporators, which are generally not employed during summer mode. The pressure of $EVAP_{AC,2}$ is controlled by the LT base compression block, which during cooling mode operates 4 to 6 bar below the INT level. The parallel compressor(s) will increase capacity and thus reduce INT pressure if additional cooling is needed. Simultaneously, the AC chilled water pumps will increase the mass flow rate through the heat exchangers. In the case of the ejector-supported system displayed in Figure 2b, a large portion of the CO_2 is lifted from LT to the INT pressure level.

The DHW storage functions as the only useful heat sink to the system during summer mode, as SH demand is lacking during high ambient temperature operations. If removal of excess heat is needed, DV_1 directs the flow towards GC_{air} for rejection towards the ambient air.

3. Methodology

3.1. Numerical Model

Detailed models of the thermal systems were created in the object-oriented programming language Modelica. The programming environment Dymola 2018 was applied to

simulate the models. The standard solver, DASSL, was used for the investigations [34]. Construction of the models was achieved by using components from the commercially available thermodynamic library TIL-Suite 3.9, developed by TLK-Thermo GmbH [35]. The TIL-Media 3.9 library was applied for the simulation of the fluids used in the models, which includes CO_2, water, propylene glycol (30% mass fraction), and air with an assumed relative humidity of 60% [36]. The TIL extensions are advanced libraries for transient simulations of fluid systems and are especially applicable for heat transfer modeling purposes, i.e., heat pumps, refrigeration, cooling, and heating systems. Among the components that are included in the library are compressors, pumps, valves, and heat exchangers. The components are connected in the oriented physical modeling interface, Dymola, to construct complex models. Data for boundary conditions, such as ambient temperatures and thermal demands, were externally imported to the model.

All investigated cases are equipped with four compressors, which were modeled by their swept volumes. Correlations for circulated mass flow rate and electric power consumption were implemented based on the data published by the manufacturer. The compressor sizes were selected based on which combination of active compressors satisfied all operating criteria in the investigated cases. Compressors 1 to 4a were defined based on compressor model 4FTE-30K, with a swept volume of 17.5 m^3h^{-1} at 50 Hz. Compressor 4b was modeled after type 4JTE-15K, with a swept volume of 9.3 m^3h^{-1} at 50 Hz, and was implemented in the alternative system designs, i.e., PC and EJ. Correlations for each compressor were implemented in the model as a function of suction and discharge conditions, in addition to the rotational speed of the frequency converter (for the VSD compressors) [33].

All expansion valves were modeled using orifice valves, where the Bernoulli equation was applied to calculate the mass flow rate as a function of pressure difference. Modulating and directional valves (MV and DV) were modeled using three-way linear directional control valves, in which inlet mass flow is split into two flows, depending on the value of the switching position. The opening of the valves is regulated by proportional-integral (PI) controllers to reach their respective setpoints temperature. MV_1 controls the flow of CO_2 through $GC_{DHW,2}$ to reach a DHW temperature of 70 °C. MV_2 and MV_3 are controlled to ensure a superheat of 10 K at the suction line of the parallel and base compression stack, respectively. The mass flow rate of each branch is calculated using a linear pressure drop relation, which is formulated based on nominal pressure loss at nominal volume flow rate [37]. Table 1 lists the characteristics and heat transfer area for the heat exchangers applied in the models.

Table 1. Heat exchangers characteristics based on commercial available components.

Label	Heat Exchanger	Type	Secondary Fluid	Heat Transfer Area [m^2]
GC_{SH}	Gas cooler	Plate	Water	16.87
$GC_{DHW,1}$	Gas cooler	Plate	Water	5.07
$GC_{DHW,2}$	Gas cooler	Plate	Water	2.73
GC_{AIR}	Gas cooler	Fin and tube	Air	4 × 297.60 *
$EVAP_{AC,1}$	Evaporator	Plate	Glycol	9.61
$EVAP_{AC,2}$	Evaporator	Plate	Glycol	7.67
$EVAP_{AIR}$	Evaporator	Fin and tube	Air	4 × 297.60 *
IHX_1	Internal heat exchanger	Plate	CO_2	0.85
IHX_2	Internal heat exchanger	Plate	CO_2	1.75

* Air-side heat transfer area, tube volume of 51.2 L.

The four air heat exchanger units, which can be applied as both evaporators and gas coolers, are modeled in the same manner independent of operation. Each unit was modeled as a fin-and-tube cross-flow heat exchanger. Haaf's correlation [38] was applied to calculate the air-side heat transfer coefficient. The heat transfer coefficient on the refrigerant side

was estimated to 2500 W m^{-2} K^{-1}. The fin efficiency of each unit was modeled after the correlation by Schmidt [39]. In evaporation mode, the setpoint of the airflow through each heat exchanger is controlled to maintain an evaporating temperature 4 K below ambient temperature. Similarly, airflow is controlled to cool the temperature of CO_2 down to 4 K above ambient temperature in gas cooler mode.

The gas coolers for SH and DHW production, AC evaporators, and internal heat exchangers were implemented using plate heat exchanger models from the TIL library. The pressure drop in each heat exchanger was approximated using quadratic correlations formulated based on nominal pressure loss at nominal volume flow rate [37]. The correlation for chevron plates developed by Huang et al. [40] was applied to calculate the coefficient of heat transfer for the single-phase fluids in the gas coolers. This correlation was also applied to calculate the heat transfer coefficient on the glycol side in each of the two AC evaporators. An ideal separator with a volume of 300 L was applied to model the liquid receiver.

The gas cooler pressure is regulated with the high pressure valve, HPV, in the system configurations presented in Figures 1 and 2a. A PI-controller continuously regulates the valve opening area to meet the setpoint for the high pressure, which is defined based on operating zones, according to the principles described by Gullo et al. [41]. Additional constraints, such as supply temperature for SH and DHW, are applied to ensure that setpoints of the system are satisfied. The minimum and maximum gas cooler running pressure is 60 and 105 bar, respectively. In the system configuration presented in Figure 2b, the ejector is applied to control the gas cooler pressure. The ejector is modeled as a Multi-ejector block based on type HP 2875, which consists of fixed-geometry ejectors of different sizes, arranged in parallel within a block and which can be enabled or disabled according to the operating conditions. The nozzle flow was modeled using correlations by Brennen [42] and continuous control of the ejector opening degree was assumed. The ejector efficiency, η, was defined according to the relations presented in Elbel and Hrnjak [43]. Furthermore, the ejector efficiency was modeled by the use of the correlations given in Equations (1) and (2), which were developed based on operational performance data made publicly available from the manufacturer. The correlations are applicable for an ejector pressure-lift range of 4 to 6 bar.

$$\eta = a + bP_m + cT_m + dP_m^2 + eP_mT_m + fT_m^2 + gP_m^2T_m + hP_mT_m^2 + iT_m^3 - \eta_{corr}(6 - P_{lift}) \quad (1)$$

where T_m [°C] and P_m [bar] represents the motive temperature and pressure, respectively. The pressure lift, P_{lift} [bar], is introduced and corrected for, within the limits of the pressure-lift range, by the means of η_{corr} given in Equation (2). Values for the correlation coefficients applied in the equations are listed in Table 2.

$$\eta_{corr} = a + bP_m + cT_m + dP_m^2 + eP_mT_m + fT_m^2 + gP_m^3 + hP_m^2T_m + iP_mT_m^2 \quad (2)$$

Table 2. Values of correlation coefficients for Equations (1) and (2), which were applied to simulate the multi-ejector efficiency (developed for the range 4–6 bar).

η (Equation (1))	η_{corr} (Equation (2))
$a = 4.258$	$a = -6.839 \times 10^{-1}$
$b = -7.943 \times 10^{-2}$	$b = 4.743 \times 10^{-2}$
$c = -1.718 \times 10^{-1}$	$c = -9.552 \times 10^{-2}$
$d = 3.902 \times 10^{-4}$	$d = -7.155 \times 10^{-4}$
$e = 0.378 \times 10^{-2}$	$e = 1.688 \times 10^{-3}$
$f = -1.348 \times 10^{-4}$	$f = 6.161 \times 10^{-4}$
$g = -2.334 \times 10^{-5}$	$g = 2.996 \times 10^{-6}$
$h = 1.780 \times 10^{-5}$	$h = -6.288 \times 10^{-6}$
$i = -2.459 \times 10^{-5}$	$i = -7.867 \times 10^{-6}$

3.2. DHW Charging Strategy

The DHW charging strategy is a key influencing factor to achieve a high overall system performance in CO_2 heat pumps [29]. The thermal storage of 6 m^3 provides a buffer that enables a high degree of flexibility with regard to operating strategy. Two different charging strategies, *leveled* and *aggressive* charging, are investigated to evaluate the influence of thermal storage operation in light of design and overall performance.

3.2.1. Leveled Charging

Charging at reduced loads has the potential to limit return temperatures from the secondary systems and, by this, enhance system performance. A control scheme that aims to reduce DHW charging load and increase charging time has been formulated based on the storage volume and the temperature span across the storage. The simplified decision tree describing the outline of the leveled control strategy algorithm to determine the DHW charging load at time i, L_i, is shown in Figure 3.

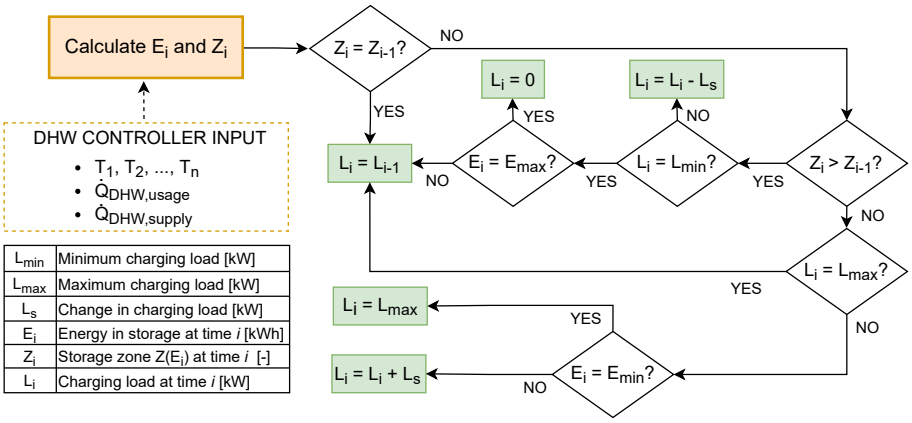

L_{min}	Minimum charging load [kW]
L_{max}	Maximum charging load [kW]
L_s	Change in charging load [kW]
E_i	Energy in storage at time *i* [kWh]
Z_i	Storage zone $Z(E_i)$ at time *i* [-]
L_i	Charging load at time *i* [kW]

Figure 3. Simplified decision tree control logic to determine DHW charging load with the leveled charging strategy.

The DHW storage is divided into six separate zones, Z, which are formulated based on the maximum available energy reservoir of the storage,E_{max}. For instance, zone 1 applies when the DHW storage has a low temperature and, thus, no useful energy reserve. Zone 6 is reached when all tanks attain a temperature of 70 °C. The energy in storage at time i,E_i, is calculated based on DHW controller input variables, which include the temperatures across the storage, $T_1 - T_n$, the rate of energy entering, $\dot{Q}_{DHW,supply}$, and exiting the storage, $\dot{Q}_{DHW,usage}$. These values are attained directly in the simulations but could easily be calculated in a real-life system as a function of measured mass flow rates and temperatures of water entering and exiting the DHW storage tanks. The zone at time i,Z_i, is further calculated to determine L_i. The minimum and maximum loads in which the heat pump can actively produce hot water, L_{min} andL_{max}, are defined as 50 kW and 110 kW, based on the load profile and the size of the heat exchangers. The step value in which the charging load increases or decreases, L_s, is fixed to 10 kW.

3.2.2. Aggressive Charging

The aggressive charging strategy represents a common practice in regards to the operation of DHW thermal storage's [29,30]. The aim of the strategy is to charge the DHW storage tanks periodically from low to high temperature, which results in charging over several periods during the day, usually at high loads and intervals of 8 to 12 h. Typically, the aggressive charging strategy is applied when DHW is produced through heat recovery, e.g., from a supermarket, as the heat source is more available for particular hours of the day [44]. In addition, heat pump operations with under-dimensioned thermal storage or

excessive DHW demands will inevitably result in aggressive charging to meet demands. The control logic for the aggressive charging strategy is shown in Figure 4.

Similar to the leveled charging strategy illustrated in Figure 3, six separate zones, Z, are applied. Also, L_{min} and L_{max} are defined as 50 kW and 110 kW, respectively. The starting point of the algorithm for the aggressive charging strategy is when the energy in the storage, E_i, reaches its minimum, E_{min}. The charging load, L_i, is set to zero when the energy in the storage reaches its maximum, E_{max}.

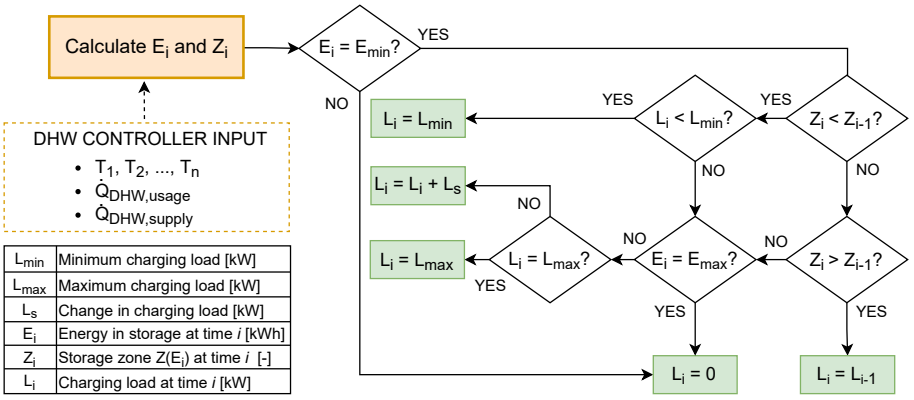

L_{min}	Minimum charging load [kW]
L_{max}	Maximum charging load [kW]
L_s	Change in charging load [kW]
E_i	Energy in storage at time *i* [kWh]
Z_i	Storage zone Z(E_i) at time *i* [-]
L_i	Charging load at time *i* [kW]

Figure 4. Simplified decision tree control logic to determine DHW charging load with the aggressive charging strategy.

3.3. Operating Range

The integrated CO_2 heat pumps have been designed with the aim of achieving high performance through system flexibility. An ambient temperature span from −15 to 35 °C has been selected to demonstrate different operating modes in a typical Scandinavian climate. The assumed SH and AC cooling loads supplied by the heat pump at different ambient temperatures are listed in Table 3. The loads have been established based on thermal demands of a medium-sized Norwegian hotel [29]. The setpoint curve for the SH water temperature is dependent on ambient conditions and is shown in Figure 5. The dimensioning supply and return temperature of chilled water are 7 and 12 °C, respectively. The values have been defined as per the industry rule-of-thumb for AC cooling in Scandinavia [45].

Table 3. Ambient temperature dependent space heating and AC cooling loads supplied by the integrated system.

Ambient temperature [°C]	−15	−10	−5	0	5	10	15	20	25	30	35
Space heating load [kW]	180	180	140	100	80	60	40	0	0	0	0
AC cooling load [kW]	0	0	0	0	0	0	0	40	80	150	220

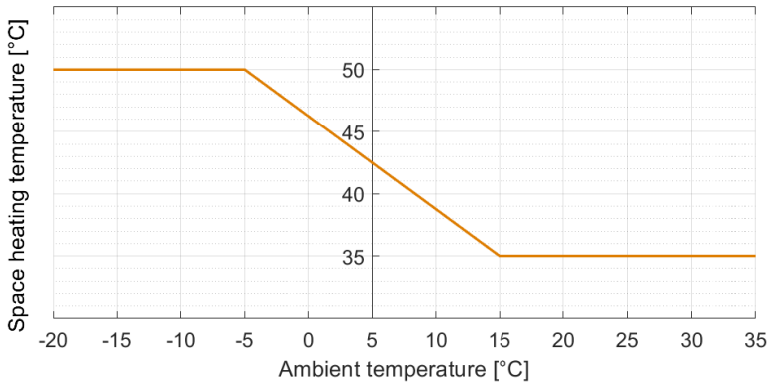

Figure 5. Set point curve for hydronic circuit for space heating depending on ambient temperature.

Four Scandinavian cities have been selected for comparisons, covering a broadest range of temperature profiles. Included in the analysis are four cities located in Central and Southern Europe to evaluate the warm climate performance potential of the designs. The climate data were obtained with the software MeteoNorm 7.1 and is based on recorded data from the period 1991–2010 [46]. The occurrences of ambient temperatures across a standard year are shown in Figure 6. A temperature bin of ±2.5 °C for given ambient temperatures has been applied.

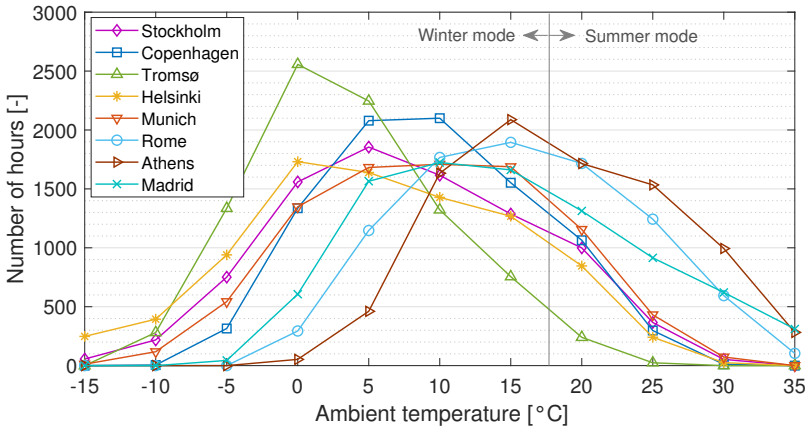

Figure 6. Number of hours per year at different ambient temperatures for the selected locations.

An hourly-dependent DHW demand profile is applied to the models to demonstrate the DHW thermal storage charging and discharging. Figure 7 depicts the DHW demand profile, which is repeated every 24 h. As for the thermal demands established for SH and AC cooling, the DHW demand profile is based on recorded operational data presented by Smitt et al. [29]. The city water temperature and DHW setpoint temperature are assumed independent of ambient conditions and have been applied to the models as constant values of 10 and 70 °C, respectively.

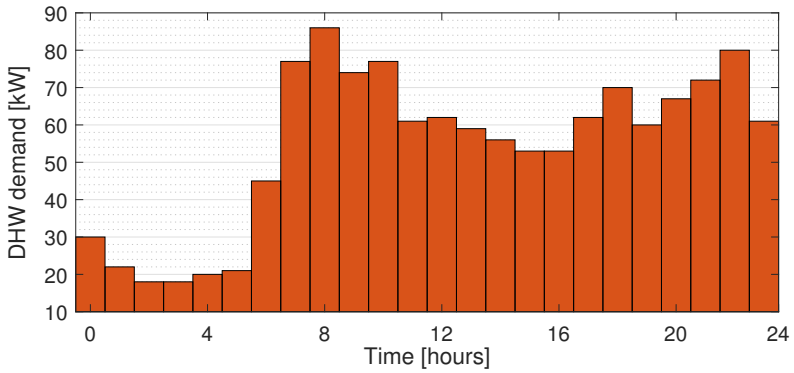

Figure 7. Domestic hot water consumption curve for the hotel, which is applied to the models.

3.4. Performance Evaluation

The overall COP of the system, hereafter referred to as COP, is applied to evaluate the performance of the system designs, and is defined in Equation (3):

$$COP = \frac{\dot{Q}_{SH} + \dot{Q}_{DHW} + \dot{Q}_{AC}}{\dot{W}} \quad (3)$$

where $\dot{Q}_{SH}$, $\dot{Q}_{DHW}$ and $\dot{Q}_{AC}$ represent SH, DHW, and AC loads, respectively, and $\dot{W}$ the electricity consumption of the compressor(s). Which terms are included at the span of ambient temperatures is given by Table 3. For instance, only the heating loads for DHW

and SH are considered during winter mode. While operating in summer mode, only DHW heating and AC cooling loads are included in the COP calculation.

3.5. Environmental Impact Evaluation

The total equivalent warming impact (TEWI) assesses both the direct and indirect emissions of greenhouse gases related to the system. Direct emissions are due to refrigerant leaks and is a function of refrigerant GWP [kg $CO_{2\text{-eq}}$·kg^{-1}] and leakage rate, L [kg]. Indirect emissions are a product of annual electric energy consumption at each location, E_e, and the CO_2 emissions associated with the process of electricity generation at each location, β [g $CO_{2\text{-eq}}$·kWh^{-1}]. The annual TEWI, $TEWI_{annual}$, is defined in Equation (4).

$$TEWI_{annual} = TEWI_{direct} + TEWI_{indirect} \quad (4)$$

$$TEWI_{direct} = GWP \cdot L \quad (5)$$

$$TEWI_{indirect} = E_e \cdot \beta \quad (6)$$

The following values were applied in the analysis:

- GWP of CO_2 = 1. GWP of existing R134a AC system = 1430 [47].
- Annual leakage rate is assumed 15% of refrigerant charge for all systems [48].
- The charge of the CO_2 systems is assumed to be 300 kg. The charge of the R134a system is assumed to be 2 kg_{134a}·$kW_{AC,max}{}^{-1}$ [48].
- Emissions associated with electricity generation at each location is given according to country values (2019) as $\beta_{Stockholm}$ = 12, $\beta_{Copenhagen}$ = 112, $\beta_{Tromsø}$ = 19, $\beta_{Helsinki}$ = 89, β_{Munich} = 350, β_{Rome} = 233, β_{Athens} = 606 and β_{Madrid} = 210 [49].

3.6. Economic Evaluation

In evaluating the proposed designs' economic viability as retrofit solutions, both initial capital cost and operational costs are considered. Cost functions were applied for all major system components, i.e., compressors, heat exchangers and valves. Equipment costs were collected from the manufacturer catalogs for specialized components, such as the ejector and the combined air evaporator/gas cooler. Table 4 lists the capital cost functions applied in the economic analysis, which are applied for full load conditions.

Table 4. Cost functions of various components [50–52].

Component	Capital Cost Function
Compressors with electrical motor	$10{,}167.5 \times \dot{W}^{0.46}$ [a]
Plate HX	$1397 \times A^{0.89}$ [a]
Fin-and-tube HXs	119,500 [b,*]
Valves	$114.5 \times \dot{m}$ [a]
Receiver	1000 [b]
Ejector	9000 [b,*]

[a] Function given in $, [b] Function given in €, * From manufacturer catalog.

Investment costs related to the secondary systems have not been considered, as the necessary components would already be in place during a retrofit. The cost of installation and additional equipment, such as the control system and piping, is assumed to be equal to 15% of the total capital cost of the system [53].

The Chemical Engineering Plant Cost Index is applied to adjust the original cost to the cost at reference year [54]. The annual average cost index (607.5) of 2019 is used as a reference. The cost of the components is adjusted according to the cost index as given by Equation (7) [55].

$$\text{Cost at reference year} = \text{original cost} \times \frac{\text{Index value for reference year}}{\text{Index value for original year}} \quad (7)$$

The economic viability of the designs is evaluated by means of the net present value (NPV) and discounted payback period (DPP), defined in Equations (8) and (10), respectively. NPV is a method to represent the discounted cash flow, which is defined as the sum of net cash flows over the plant economic life, N, calculated as

$$NPV = C_i + \sum_{t=0}^{N} \frac{C_e(1+r_e)^t}{(1+r_d)^t} \quad (8)$$

where r_d is the average annual effective discount rate (cost of money), and r_e is the general inflation rate of electricity prices. The net cash flow is represented by the initial investment cost, C_i, and the sum of all operational incomes over the system's lifetime, which in this analysis amount to the saved electricity expenses, C_e. The latter is defined in Equation (9).

$$C_e = p\left(\frac{E_{SH}+E_{DHW}}{\eta_{el}} + \frac{E_{AC}}{COP_{AC,al}} - \frac{E_{SH}+E_{DHW}+E_{AC}}{COP}\right) \quad (9)$$

An existing reference system (capital cost = 0), consisting of an electric boiler and an alternative standard AC cooling unit, is applied for the analysis. It is assumed that all SH and DHW energy requirements, E_{SH} and E_{DHW}, are covered by the electric boiler, while all cooling energy, E_{DHW}, is covered by the alternative AC chiller.

The DPP, defined in Equation (10), determines the time from investment to return of the invested capital. DDP is calculated by identifying the year, Y_n, in which the proceeding cumulative net cash flow (NCF), $\sum_{t=0}^{n} NCF_n$, turns positive. The exact time of return is found by accounting for the discounted value of the cash flow of the next period, NCF_{n+1}.

$$DPP = Y_n + \frac{abs(\sum_{t=0}^{n} NCF_n)}{NCF_{n+1}} \quad (10)$$

Data applied in the economic analysis are listed below.

- The general inflation rate is r_e = 2.5% [53].
- The average annual effective discount rate is r_d = 10% [53].
- The plant economic life is N = 15 years [52,53].
- The electric boiler efficiency is η_{el} = 95% [56].
- The European seasonal energy efficiency ratio (ESEER) of the alternative R134a AC cooling system is ESEER = $COP_{AC,al}$ = 2.52 (from manufacturer catalog).
- Costs related to system maintenance and operation have been neglected [52,53].

4. Results and Discussion

4.1. System Performance and Operation

Transient simulations were conducted for the purposed CO_2 systems with the boundary conditions and control schemes described in Section 3. Figure 8 compares the COP of the investigated designs as a function of ambient temperature and charging strategy. Naturally, the COP for all designs increases with ambient temperature as the pressure ratio of the compressors diminishes. At 20 °C, the COP of all designs increases considerably to values in the range of 7.3 to 7.6 and 5.8 to 6.3 for leveled and aggressive charging, respectively. This is explained by the presence AC cooling demand during high ambient temperatures, which enables combined heat pump and chiller operations. The COP of all designs are gradually reduced from 25 °C, due to the increase in AC cooling loads relative to the DHW production load.

Figure 8 clearly illustrates that the system with the ejector arrangement, EJ, outperforms both SC and PC, independent of charging strategy. A more significant benefit is achieved from the ejector at ambient temperatures above 15 °C, where the performance is enhanced by up to 20% and 14% compared with SC and PC, respectively. Moreover, leveled charging results typically increased COP compared with aggressive charging due to continuous DHW charging during all operational hours. In contrast, DHW production

transpires in about 60% of the operation when aggressive charging. The most considerable difference in performance in terms of charging strategy occurs at 20 °C, in which leveled charging enhances COP considerably. As observed in the figure, an increase in COP of more than 20% is achieved for all investigated designs. DHW is continuously produced when applying the leveled charging strategy, and thus, there is no need to dump heat to the ambient. In contrast, DHW is periodically produced at high loads when applying aggressive charging, resulting in heat rejection to the ambient and reduced COP compared with leveled charging.

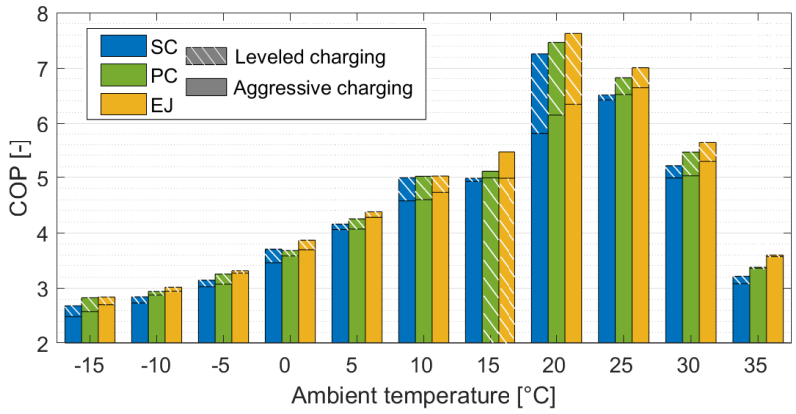

Figure 8. COP as a function of ambient temperature for the investigated designs when applying the aggressive DHW charging strategy.

The power consumption of the compressors is illustrated in Figure 9; also included in the figure is the arrangement of the pivoting compressors for the PC and EJ designs. The data shown in Figure 9 demonstrate the behavior of the system when the leveled charging strategy is applied. Generally, the SC design attains higher power consumption due to a slight increase in compressor pressure ratio compared to PC and EJ, which are both equipped with optional pivoting parallel compressors. However, the power consumption of all investigated designs are nearly equal in the temperature range from 10 to 15 °C. This is explained by the relatively large DHW demand, which results in a reduced CO_2 gas cooler outlet temperature, and thus less vapor formation after expansion to the liquid receiver. Consequently, solely base compressor 1 is employed to cover the heating demand in all investigated designs.

Both PC and EJ designs rely heavily on the base compressors during low ambient temperature operations from −15 to 5 °C. Compressor 2 is in both designs employed as a base compressor. The opposite trend is observed at ambient temperatures of 20 °C and above, as the pivoting compressors (2 and 3) are integrated in the parallel compressors section. Thus, the pivoting compressors enable flexible and efficient operation of integrated CO_2 systems over a wide range of ambient temperatures. In addition, a smaller total compressor capacity is needed when applying the pivoting option, as illustrated by the reduced swept volume of compressor 4 (b) in PC and EJ, the value of which is given in Section 3.1. Thus, pivoting compressors have the potential to reduce both investment and operational costs when compared with a single-stage compression system, especially for installations of considerable size [57].

Figure 10 presents the ejector efficiency and entrainment ratio for the EJ system design when applying both the leveled and aggressive charging strategy. The average ejector efficiency is recorded in the range of 0.0 to 0.34 when leveled charging is applied. The low values of efficiency occur at 10 and 15 °C, as the efficiency function (Equation (1)) advances towards zero when the CO_2 temperature before expansion is low. In the case of aggressive charging, the ejector operates in an average efficiency range of 0.17 to 0.28. Moreover, it can be observed that more liquid is entertained when applying the aggressive charging strategy. Thus, the overall benefit of the ejector is more significant when applying the aggressive

charging strategy, explained by the elevated gas cooler outlet temperature during this mode of operations.

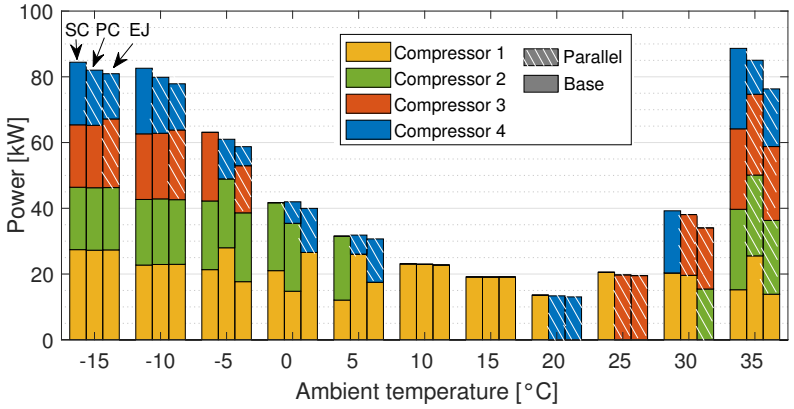

Figure 9. Electric power consumption and arrangement of the compressors when applying the leveled charging strategy. The three different bars at each temperature interval represents the designs of SC, PC, and EJ.

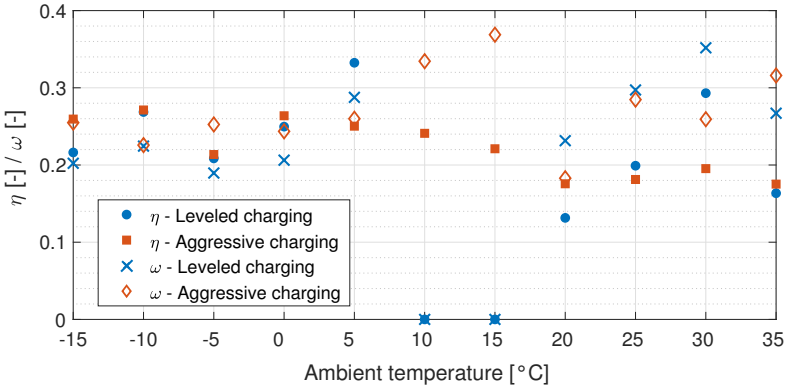

Figure 10. Ejector efficiency (η) and entrainment ratio (ω) for the EJ design when applying the leveled and aggressive charging strategy.

As illustrated in Figure 7, a constant DHW demand pattern was selected for this investigation. However, fluctuations will occur in real-life systems due to variation in hotel guest load, which will highly influence the magnitude of DHW demand peaks. Thus, it is likely that the CO_2 system is occasionally forced to operate with aggressive charging to fulfill excessive DHW demands. An alternative scenario is heat pump operations during periods when the guest load is low. In these instances, a surplus of stored DHW will result in periods of operation without DHW production, and as a consequence, elevated gas cooler outlet temperatures. Therefore, the advantages of the ejector are likely more prominent than what was achieved in this investigation. This may speak for applying ejector technology in CO_2 heat pump and chiller systems for hotels, despite the fact that the benefits and influence on COP are limited when applying the leveled charging strategy.

4.2. Annual Energy Consumption and Environmental Impact

The annual COP and energy consumption of the investigated solutions for different locations are listed in Table 5. The EJ design demonstrated superior performance, followed by PC and SC for all locations independent of charging strategy. The COP at the locations were improved by 3.1% (Copenhagen) to 4.1% (Athens) when comparing EJ to SC (leveled charging strategy). Similar results were obtained with the aggressive charging strategy, in which the COP at each location increased by 4.7% (Stockholm) to 6.9% (Athens) with the EJ design.

Table 5. Annual COP, energy usage, and emissions (TEWI) of the investigated systems at the selected locations when applying the leveled charging strategy.

Strategy	Variable/Location	Annual COP [-]			Annual Energy Usage [MWh· y^{-1}]			Annual Emissions [Tonne $CO_{2\text{-eq}}$· y^{-1}]		
		SC	PC	EJ	SC	PC	EJ	SC	PC	EJ
Leveled charging	Stockholm	4.68	4.75	4.85	278.65	277.19	268.32	3.39	3.37	3.26
	Copenhagen	4.86	4.92	5.01	240.64	240.90	233.61	27.00	27.02	26.21
	Tromsø	4.12	4.16	4.27	333.56	331.32	319.54	6.38	6.34	6.11
	Helsinki	4.48	4.55	4.64	311.25	308.52	298.82	27.74	27.50	26.64
	Munich	4.86	4.93	5.03	253.35	252.57	244.84	88.72	88.44	85.73
	Rome	5.49	5.61	5.71	206.74	205.60	199.60	48.21	47.95	46.55
	Athens	5.62	5.76	5.85	213.01	210.34	203.40	129.18	127.51	123.30
	Madrid	5.19	5.30	5.40	237.44	235.76	227.15	49.91	49.55	47.75
Aggressive charging	Stockholm	4.43	4.45	4.64	293.56	290.39	276.11	3.57	3.53	3.36
	Copenhagen	4.50	4.61	4.80	254.05	252.64	240.35	28.50	28.34	26.96
	Tromsø	3.88	3.96	4.14	349.94	345.25	328.18	6.69	6.61	6.28
	Helsinki	4.17	4.28	4.46	327.84	323.07	307.26	29.22	28.80	27.39
	Munich	4.51	4.65	4.82	267.18	264.57	251.45	93.56	92.64	88.05
	Rome	5.03	5.20	5.40	218.57	217.10	206.23	50.97	92.64	88.05
	Athens	5.19	5.34	5.55	224.95	221.68	209.86	136.36	134.38	127.22
	Madrid	4.82	4.94	5.15	250.07	247.09	234.02	52.56	51.94	49.19

The results in Table 5 illustrate that the ambient temperatures at each location highly influence annual energy consumption. The lowest annual energy consumption was achieved in the warmest city, Rome, where the range of consumption was recorded from 199.60 to 218.57 MWh· y^{-1} for all investigated cases. In the coldest city, Tromsø, the annual energy consumption was found to approximately 60% higher, in the range of 319.54 to 349.94 MWh· y^{-1}. When comparing results obtained with the two different charging strategies, it can be concluded that the highest annual COPs were achieved when applying the leveled charging strategy. Furthermore, results from aggressive charging with the best design in terms of COP, EJ, are comparable to the COPs obtained with SC when applying leveled charging. For instance, Munich achieved an annual COP of 4.86 with SC (leveled charging) and 4.82 with EJ (aggressive charging). Thus, DHW control strategy rather than system design appears to be the largest influence factor on COP and energy consumption at each investigated location.

The annual global warming impact from each system, in terms ton $CO_{2\text{-eq}}$ emission, is included in Table 5. A large variation in emission is observed at the different locations, in which Stockholm displays the lowest emission values of approximately 3 tons $CO_{2\text{-eq}}$ per year. This amounts to approximately 2.5% of the related emissions in Athens, which are between 123 to 129 tonne per year, dependent on system design. Energy savings and emission reductions associated with installing the SC design in place of the existing solution (boiler + separate AC chiller) are shown in Figure 11. The largest reduction of emissions is achieved in Athens and Rome, where between 310 to 380 tonnes $CO_{2\text{-eq}}$ can be prevented on an annual basis. In terms of energy utilization, the largest savings were achieved in the Scandinavian locations, ranging from 850 to 1000 MWh·y^{-1}. Information related to energy savings and emission reduction for PC and EJ can be found in Appendix Table A1.

4.3. Economical Analysis

The total capital cost of the considered designs is listed in Table 6. As can be observed from the table, the investment cost related to compressors and heat exchanger represent the majority of the capital cost in all cases. When considering all designs, the total capital cost for each of the suggested designs is within a range of ±2.5%.

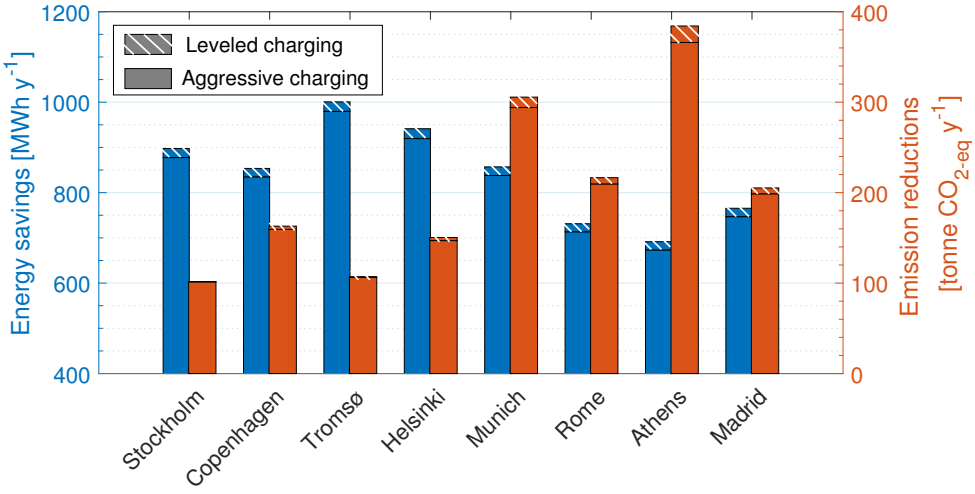

Figure 11. Annual energy savings and reduction in related emissions (TEWI) of SC design in relation to the reference thermal system. The eight selected locations are investigated when applying both the leveled and aggressive charging strategy.

Table 6. Total equipment investment cost of the CO_2 designs with single-stage compression (SC), parallel compression (PC), and ejector-supported parallel compression (EJ).

Investment	**Capital Cost [k€]**		
	SC	**PC**	**EJ**
Compressors	174.6	169.2	169.2
Heat exchangers	171.7	174.2	174.2
Valves/receiver/ejector	2.3	2.4	11.2
Installation and additional equipment (15%)	50.6	51.9	53.2
Total	**399.2**	**397.7**	**407.8**

The DPP and NPV for the SC design at different electricity prices are shown in Figures 12 and 13. The results for the eight locations have been divided into two separate plots for each economic comparison. Moreover, the influence of both the leveled and the aggressive charging strategies is included in the figures.

As seen from Figure 12, aggressive charging prolongs the DPP for all locations with approximately 0.7 to 1.5 years at 0.06 €·kWh^{-1}. As the electricity price increases, the benefit of the charging strategy on DPP is reduced to a few months at 0.20 €·kWh^{-1}. However, the economic benefit at high electricity prices for each location is more evident when evaluating NPV. As shown in Figure 13, the difference in NPV for leveled and aggressive charging varies between 0.07 and 0.1 M€ at an electricity price 0.20 €·kWh^{-1} for all evaluated locations. Thus, it is possible to save up to 25% of the initial investment cost by applying the leveled charging strategy.

The DPP for the locations drops significantly from a range of 9 to 16 to around 3 years as the electricity price increases from 0.06 to 0.20 €·kWh^{-1}. Similarly, the NPV for the locations varies between 0 and 0.02 M€ and 0.8 and 1.4 M€ at the selected range of electricity prices (Figure 13). Locations with low ambient temperatures and low annual COP display the shortest DPP and highest NPV, which is in contrast to COP values listed in Table 5. This is explained by the large savings in SH energy achieved at locations characterized by low ambient temperatures, such as Tromsø and Helsinki, where the alternative would be application of an electric boiler. The best performing location in the operational analysis, Athens, has the longest DPP with a break-even point between 3.3 and 16+ years. The NPVs for Athens, Rome, and Madrid are close to and below zero at an electricity price of 0.06 €·kWh^{-1}, and thus not economically viable investments. However, the actual electricity price at the locations must be considered to give a more accurate evaluation. Generally, the electricity price for commercial actors in Scandinavia is in the

range of 0.06 to 0.08 €·kWh^{-1}, while the equivalent electricity price in Germany (Munich), Italy (Rome), and Athens (Greece) is typically at values of 0.18, 0.15, and 0.10 €·kWh^{-1}, respectively [58]. If only considering results in which leveled charging is applied, DPPs of approximately 3 (Munich), 4.5 (Rome), and 7.5 years (Athens) and NPVs in the range of 0.25 to 0.95 M€ were achieved when considering typical electricity prices at the locations. Thus, integrated heating and cooling systems with CO_2 can be efficient, cost-effective and environmentally friendly when applied in warmer European climates.

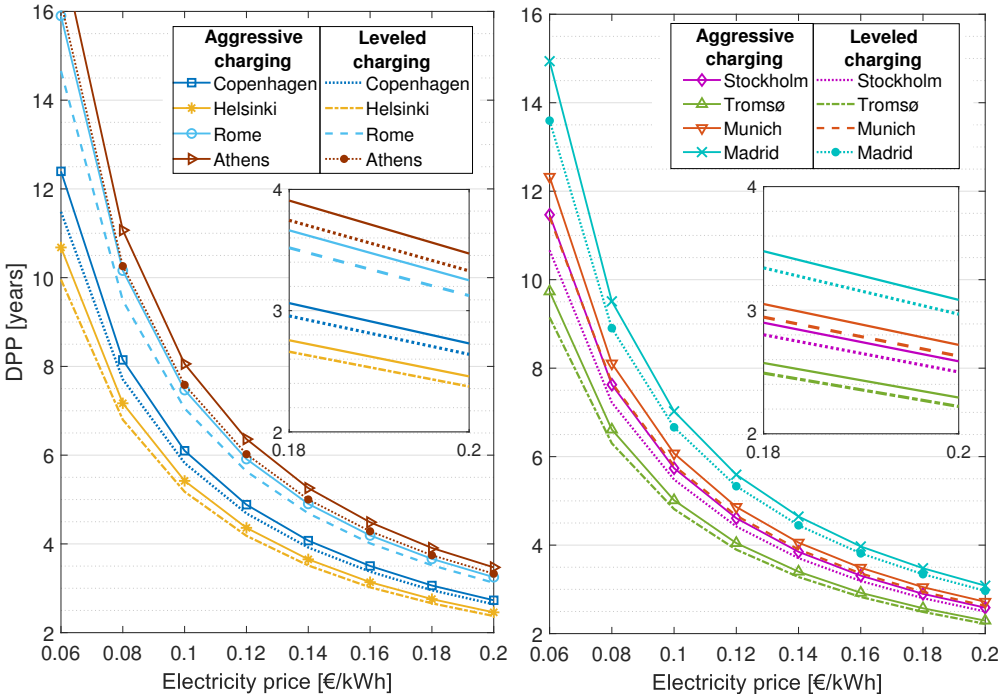

Figure 12. Discounted payback period for selected cities with the SC design at different electricity prices when applying the leveled and aggressive charging strategy.

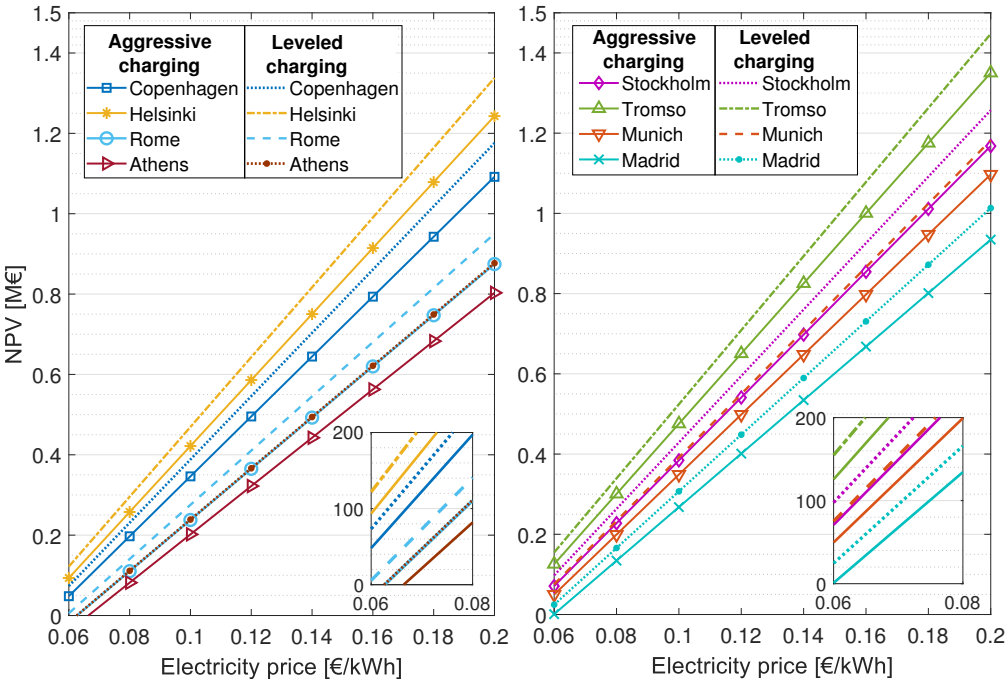

Figure 13. Net present value for selected cities with the SC design at different electricity prices when applying the leveled and aggressive charging strategy.

The DPP for the Scandinavian locations is 9 to 12.5 years at 0.06 €·kWh^{-1}. At an electricity price of 0.08 €·kWh^{-1}, DPP and NPV for the Scandinavian locations are between 6.3 to 7.7 years. This is considered high when related to the rule-of-thumb for heat pump investments within Scandinavia, which generally points to a payback time of 5 years or less. However, the NPV for this investment for the Scandinavian locations is between 0.23 to 0.34 M€. Thus, profits of approximately 50–85% of the initial investment can be gained over the systems' economic lifetime. Integrated CO_2 heat pumps and chillers are, therefore, cost-efficient compared to more conventional approaches, including electric boilers or district heat in combination with separate chillers for AC. Nevertheless, when compared to HFO systems for hotels, CO_2 integrated systems still face a challenge in terms of the high investment cost. Throughout history, new and supposedly safe refrigerants have been introduced (CFC, HCFC and HFC) as an alternative to natural refrigerants. All of them have eventually been phased out as their impact on human health and the environment is revealed. In later years, research suggests that the decomposition products from HFO refrigerants are harmful. Moreover, the research community is investing significant efforts to uncover all unknown side effects of applying HFOs [12,13]. Thus, when factoring in environmental concerns, and the fact that future regulations regarding HFOs are unknown and thus pose an economic risk for the hotel owner, one can argue that the somewhat high investment costs related to integrated CO_2 systems in Scandinavia are justified.

Tables 7 and 8 list the NPV and DPP at the selected locations when the PC and EJ system designs are applied, respectively. Results for the entire range of electricity prices can be found in Tables A2 and A3. Both PC and EJ display comparable results to SC (Figures 12 and 13). However, the economic data obtained with PC illustrate a slightly better NPV and DPP at all locations when applying the leveled charging strategy.

In contrast to the results presented in Section 4.2, in which EJ was found to be the superior solution in terms of annual COP and energy consumption, the economical analysis reveals that PC is better when considering overall system cost. However, results from both the operational and the economic evaluation show that improving the DHW charging strategy is the least expensive and most efficient measure to enhance the performance of integrated CO_2 systems.

Table 7. Net present value (NPV) and discounted payback period (DPP) for selected cities with the PC design at different electricity prices when applying the leveled and aggressive charging strategy.

Strategy	Variable/Location	NPV at Selected Electricity Prices [M€]			DPP at Selected Electricity Prices [years]		
		0.06	**0.14**	**0.20**	**0.06**	**0.14**	**0.20**
Leveled charging	Stockholm	0.10	0.77	1.27	10.5	3.7	2.5
	Copenhagen	0.08	0.71	1.18	11.4	3.9	2.6
	Tromsø	0.16	0.90	1.46	9.0	3.2	2.2
	Helsinki	0.13	0.83	1.35	9.8	3.5	2.3
	Munich	0.08	0.71	1.19	11.3	3.9	2.6
	Rome	0.01	0.55	0.96	14.4	4.6	3.1
	Athens	<0	0.50	0.89	15<	4.9	3.3
	Madrid	0.03	0.60	1.02	13.4	4.4	2.9
Aggressive charging	Stockholm	0.08	0.71	1.18	11.3	3.8	2.6
	Copenhagen	0.05	0.65	1.10	12.2	4.0	2.7
	Tromsø	0.13	0.84	1.37	9.6	3.4	2.3
	Helsinki	0.10	0.76	1.26	10.5	3.6	2.4
	Munich	0.05	0.66	1.11	12.1	4.0	2.7
	Rome	<0	0.50	0.89	15<	4.8	3.2
	Athens	<0	0.45	0.82	15<	5.2	3.4
	Madrid	0.01	0.54	0.95	14.6	4.6	3.0

Table 8. Net present value (NPV) and discounted payback period (DPP) for selected cities with the EJ design at different electricity prices when applying the leveled and aggressive charging strategy.

Strategy	Variable/Location	NPV at Selected Electricity Prices [k€]			DPP at Selected Electricity Prices [years]		
		0.06	**0.14**	**0.20**	**0.06**	**0.14**	**0.20**
Leveled charging	Stockholm	0.10	0.77	1.27	10.8	3.7	2.5
	Copenhagen	0.07	0.71	1.18	11.7	4.0	2.7
	Tromsø	0.15	0.90	1.46	9.2	3.3	2.2
	Helsinki	0.12	0.82	1.35	10.1	3.5	2.4
	Munich	0.07	0.71	1.19	11.6	3.9	2.7
	Rome	0.00	0.55	0.96	14.9	4.7	3.2
	Athens	<0	0.50	0.89	15.0	5.0	3.4
	Madrid	0.02	0.59	1.02	13.8	4.5	3.0
Aggressive charging	Stockholm	0.07	0.71	1.19	11.5	3.9	2.6
	Copenhagen	0.05	0.65	1.11	12.5	4.1	2.7
	Tromsø	0.13	0.84	1.38	9.7	3.4	2.3
	Helsinki	0.10	0.77	1.27	10.7	3.6	2.5
	Munich	0.05	0.66	1.12	12.4	4.1	2.7
	Rome	<0	0.50	0.89	15.0	4.9	3.3
	Athens	<0	0.45	0.82	15.0	5.3	3.5
	Madrid	0.00	0.55	0.96	14.9	4.6	3.1

5. Conclusions

In this paper, three different designs of integrated CO_2 systems with thermal storage for hotels were evaluated through an energetic and economic analysis. The investigated designs were standard single-stage compression (SC), parallel compression (PC), and ejector-supported parallel compression (EJ). The performance of the systems was numerically investigated by implementing two separate DHW charging strategies: aggressive and leveled charging. In addition, variations in loads, ambient temperatures, and setpoints were applied to each numerical model. Evaluations of the annual efficiency, emissions, energy performance, net present value, and discounted payback period were carried out at eight different locations, ranging from Scandinavia to the Mediterranean.

The main conclusions drawn from this investigation are as follows.

- The EJ design demonstrated enhanced annual performance, followed by PC and SC, at all locations independent of charging strategy. Annual COPs of 4.27 to 5.03 were achieved at the location in central Europe and Scandinavia. In the Mediterranean locations, Annual COPs in the range of 5.40 to 5.70 were obtained. Considerable reductions in both related emissions and energy consumption were achieved at all locations.
- The highest annual COPs were achieved when applying the leveled charging strategy, independent of design. An increase in COPs of up to 7.3% was attained compared to the aggressive charging strategy. Thus, control of the DHW charging is a larger influencing factor on performance than system designs.
- DPP and NPV for the Scandinavian locations were found to be between 6.3 to 7.7 years and 0.23 to 0.34 M€ at typical Scandinavian electricity prices. Hotels in temperate and Mediterranean climates obtained DPPs of approximately 3 and 4.5 to 7.5 years, respectively, and NPVs in the range of 0.25 to 0.95 M€. Thus, integrated heating and cooling systems with CO_2 can be an efficient, cost-effective and environmentally friendly solution for hotels located in temperate and Mediterranean locations.

Integrated CO_2 systems have proven to be efficient and sustainable alternatives for hotel applications. However, high investment cost decelerates the rate of installation for these type of solutions. History has shown that potential harmful refrigerants are eventually heavily regulated and even banned. As a result, HFO alternatives may pose an economic risk for hotel owners. Thus, the somewhat high investment costs of integrated CO_2 systems can be justified. Further research is necessary to establish integrated CO_2

systems as a competitive alternative to traditional synthetic refrigeration systems. From this study, it can be concluded that improving the DHW charging strategy is the least expensive and most efficient measure to enhance the performance of integrated CO_2 systems.

Author Contributions: Conceptualization, S.S., Á.P. and A.H.; methodology, S.S. and Á.P.; software, S.S.; investigation, S.S.; writing—original draft preparation, S.S. and Á.P.; writing—review and editing, S.S., Á.P. and A.H.; visualization, S.S.; supervision, Á.P. and A.H. All authors have read and agreed to the published version of the manuscript.

Funding: This research received no external funding.

Institutional Review Board Statement: Not applicable.

Informed Consent Statement: Not applicable.

Conflicts of Interest: The authors declare no conflict of interest.

Nomenclature

Symbols

β	CO_2 emission factors [g $CO_{2\text{-eq}}$·kWh^{-1}]
η	efficiency [-]
C	cost [€]
E	energy [kWh]
L	leakage rate [%]
N	plant economic life [years]
P	pressure [bar]
p	electricity price [€·kWh^{-1}]
$\dot{Q}$	heat [kW]
r	rate [%]
T	temperature [°C]

Subscript

AC	air-conditioning
al	alternative
corr	corrected
d	discount
DHW	domestic hot water
e	electricity
el	electric boiler
eq	equivalent
i	investment
lift	pressure lift
m	motive
SH	space heating

Abbreviations

AC	air-conditioning
CFC	chlorofluorocarbons
CO_2	carbon dioxide
COP	coefficient of performance
DHW	domestic hot water
DPP	discounted payback period
DV	directional valve
EJ	ejector-supported parallel compression
ESEER	European seasonal energy efficiency ratio
EVAP	Evaporator
FGT	flash gas tank
GC	gas cooler
GWP	global warming potential
HCFC	hydrochlorofluorocarbons

HFC	hydrofluorocarbons
HFO	hydrofluoroolefins
HX	heat exchanger
IHX	internal heat exchanger
INT	intermediate temperature
LT	low temperature
MV	modulating valve
NCF	net cash flow
NPV	net present value
PC	parallel compression
PI	proportional–integral
SC	single-stage compression
SH	space heating
TEWI	total equivalent warming impact
TFA	trifluoroacetic acid
VSD	variable speed drive

Appendix A

Table A1. Annual energy savings and emission reductions (TEWI) of the investigated systems in relation to the reference thermal system. The eight selected locations are listed when applying both the leveled and aggressive charging strategy.

Strategy	Variable/Location	Annual Energy Savings [MWh· y^{-1}]		Annual Emission Reduction [Tonne $CO_{2\text{-eq}}$· y^{-1}]	
		PC	EJ	PC	EJ
Leveled charging	Stockholm	901.97	908.64	101.83	102.02
	Copenhagen	856.32	861.78	163.26	164.69
	Tromsø	1005.47	1014.84	107.14	107.55
	Helsinki	947.00	954.30	151.16	152.67
	Munich	860.54	866.28	307.12	311.84
	Rome	735.52	739.52	217.81	220.14
	Athens	697.00	701.46	389.25	396.15
	Madrid	770.38	776.34	206.61	209.66
Aggressive charging	Stockholm	884.03	896.07	101.46	101.77
	Copenhagen	839.85	850.18	160.10	162.64
	Tromsø	987.30	1002.01	106.53	107.14
	Helsinki	927.71	941.19	148.15	150.76
	Munich	843.74	854.70	297.05	305.47
	Rome	718.33	727.00	211.12	215.68
	Athens	679.56	688.63	371.81	384.47
	Madrid	753.48	763.76	200.68	205.58

Table A2. Net present value (NPV) and discounted payback period (DPP) for selected cities with the EJ design at different electricity prices when applying the leveled and aggressive charging strategy.

Strategy	Variabl/Locatione	NPV at Selected Electricity Prices [M€]								DPP at Selected Electricity Prices [years]							
		0.06	**0.08**	**0.10**	**0.12**	**0.14**	**0.16**	**0.18**	**0.20**	**0.06**	**0.08**	**0.10**	**0.12**	**0.14**	**0.16**	**0.18**	**0.20**
Leveled charging	Stockholm	0.10	0.26	0.43	0.60	0.77	0.93	1.10	1.27	10.8	7.3	5.5	4.5	3.7	3.2	2.8	2.5
	Copenhagen	0.07	0.23	0.39	0.55	0.71	0.86	1.02	1.18	11.7	7.8	5.9	4.8	4.0	3.4	3.0	2.7
	Tromsø	0.15	0.34	0.53	0.72	0.90	1.09	1.28	1.46	9.2	6.4	4.9	3.9	3.3	2.9	2.5	2.2
	Helsinki	0.12	0.30	0.47	0.65	0.82	1.00	1.18	1.35	10.1	6.9	5.2	4.2	3.5	3.0	2.7	2.4
	Munich	0.07	0.23	0.39	0.55	0.71	0.87	1.03	1.19	11.6	7.8	5.9	4.7	3.9	3.4	3.0	2.7
	Rome	0.00	0.14	0.27	0.41	0.55	0.68	0.82	0.96	14.9	9.6	7.1	5.7	4.7	4.1	3.6	3.2
	Athens	<0	0.11	0.24	0.37	0.50	0.63	0.76	0.89	15<	10.4	7.7	6.1	5.0	4.3	3.8	3.4
	Madrid	0.02	0.17	0.31	0.45	0.59	0.74	0.88	1.02	13.8	9.0	6.7	5.4	4.5	3.8	3.4	3.0
Aggressive charging	Stockholm	0.07	0.23	0.39	0.55	0.71	0.87	1.03	1.19	11.50	7.6	5.7	4.6	3.9	3.3	2.9	2.6
	Copenhagen	0.05	0.20	0.35	0.50	0.65	0.81	0.96	1.11	12.50	8.2	6.1	4.9	4.1	3.5	3.1	2.7
	Tromsø	0.13	0.31	0.49	0.67	0.84	1.02	1.20	1.38	9.70	6.6	5.0	4.0	3.4	2.9	2.6	2.3
	Helsinki	0.10	0.26	0.43	0.60	0.77	0.94	1.10	1.27	10.70	7.2	5.4	4.4	3.6	3.1	2.8	2.5
	Munich	0.05	0.20	0.36	0.51	0.66	0.81	0.97	1.12	12.40	8.1	6.1	4.9	4.1	3.5	3.1	2.7
	Rome	<0	0.11	0.24	0.37	0.50	0.63	0.76	0.89	15<	10.2	7.5	5.9	4.9	4.2	3.7	3.3
	Athens	<0	0.08	0.21	0.33	0.45	0.58	0.70	0.82	15<	11.1	8.0	6.4	5.3	4.5	3.9	3.5
	Madrid	0.00	0.14	0.27	0.41	0.55	0.68	0.82	0.96	14.90	9.5	7.0	5.6	4.6	4.0	3.5	3.1

Table A3. Net present value (NPV) and discounted payback period (DPP) for selected cities with the PC design at different electricity prices when applying the leveled and aggressive charging strategy.

Strategy	Variable/Location	NPV at Selected Electricity Prices [M€]								DPP at Selected Electricity Prices [years]							
		0.06	**0.08**	**0.10**	**0.12**	**0.14**	**0.16**	**0.18**	**0.20**	**0.06**	**0.08**	**0.10**	**0.12**	**0.14**	**0.16**	**0.18**	**0.20**
Leveled charging	Stockholm	0.10	0.27	0.43	0.60	0.77	0.93	1.10	1.27	10.5	7.1	5.4	4.4	3.7	3.2	2.8	2.5
	Copenhagen	0.08	0.23	0.39	0.55	0.71	0.87	1.02	1.18	11.4	7.6	5.8	4.6	3.9	3.3	2.9	2.6
	Tromsø	0.16	0.34	0.53	0.72	0.90	1.09	1.27	1.46	9.0	6.2	4.8	3.9	3.2	2.8	2.5	2.2
	Helsinki	0.13	0.30	0.48	0.65	0.83	1.00	1.18	1.35	9.8	6.7	5.1	4.1	3.5	3.0	2.6	2.3
	Munich	0.08	0.24	0.40	0.56	0.71	0.87	1.03	1.19	11.3	7.6	5.7	4.6	3.9	3.3	2.9	2.6
	Rome	0.01	0.15	0.28	0.42	0.55	0.67	0.82	0.96	14.4	9.4	7.0	5.6	4.6	4.0	3.5	3.1
	Athens	<0	0.12	0.25	0.37	0.50	0.63	0.76	0.89	15<	10.1	7.5	5.9	4.9	4.2	3.7	3.3
	Madrid	0.03	0.17	0.31	0.46	0.60	0.74	0.88	1.02	13.4	8.8	6.6	5.3	4.4	3.8	3.3	2.9
Aggressive charging	Stockholm	0.08	0.23	0.39	0.55	0.71	0.87	1.02	1.18	11.3	7.5	5.7	4.5	3.8	3.3	2.9	2.6
	Copenhagen	0.05	0.20	0.35	0.50	0.65	0.80	0.95	1.10	12.2	8.0	6.0	4.8	4.0	3.5	3.0	2.7
	Tromsø	0.13	0.31	0.48	0.66	0.84	1.01	1.19	1.37	9.6	6.5	4.9	4.0	3.4	2.9	2.5	2.3
	Helsinki	0.10	0.26	0.43	0.60	0.76	0.93	1.09	1.26	10.5	7.0	5.3	4.3	3.6	3.1	2.7	2.4
	Munich	0.05	0.21	0.36	0.51	0.66	0.81	0.96	1.12	12.1	8.0	6.0	4.8	4.0	3.4	3.0	2.7
	Rome	<0	0.12	0.24	0.37	0.50	0.63	0.76	0.89	15<	10.0	7.4	5.8	4.8	4.1	3.6	3.2
	Athens	<0	0.09	0.21	0.33	0.45	0.57	0.70	0.82	15<	10.9	7.9	6.3	5.2	4.4	3.9	3.4
	Madrid	0.01	0.14	0.28	0.41	0.54	0.69	0.81	0.95	14.6	9.3	6.9	5.5	4.6	3.9	3.4	3.0

References

1. UNFCCC. The Paris Agreement, 2021 United Nations Framework Convention on Climate Change. Available online: https://unfccc.int/process-and-meetings/the-paris-agreement/the-paris-agreement (accessed on 23 June 2021).
2. Ritchie, H. *Sector by Sector: Where Do Global Greenhouse Gas Emissions Come from?* Our World in Data: Oxford, UK, 2020. Available online: https://ourworldindata.org/ghg-emissions-by-sector#licence (accessed on 23 June 2021).
3. Eurostat. Final Energy Consumption by Sector. 2017. Available online: https://ec.europa.eu/eurostat/databrowser/view/ten00124/default/table?lang=en (accessed on 20 June 2021).
4. Economidou, M.; Atanasiu, B.; Despret, C.; Maio, J.; Nolte, I.; Rapf, O. *Europe's Buildings under the Microscope. A Country-by-Country Review of the Energy Performance of Buildings*; Buildings Performance Institute Europe (BPIE): Brussels, Belgium, 2011; pp. 35–36.
5. European Commission (EC). Action Plan for Energy Efficiency: Realising the Potential, Communication from the Commission, COM (2006) 545 Final. 2006. Available online: https://eur-lex.europa.eu/legal-content/EN/TXT/PDF/?uri=CELEX:52006DC0545&from=EN (accessed on 23 June 2021).
6. UNWTO. *Baseline Report on the Integration of Sustainable Consumption and Production Patterns into Tourism Policies*; Technical Report; United Nations World Tourism Organization: Madrid, Spain, 2019. Available online: https://www.e-unwto.org/ (accessed on 24 June 2021).
7. Dalton, G.; Lockington, D.; Baldock, T. Feasibility analysis of stand-alone renewable energy supply options for a large hotel. *Renew. Energy* **2008**, *33*, 1475–1490. [CrossRef]
8. Werner, S. District heating and cooling in Sweden. *Energy* **2017**, *126*, 419–429. [CrossRef]
9. Lund, H.; Möller, B.; Mathiesen, B.V.; Dyrelund, A. The role of district heating in future renewable energy systems. *Energy* **2010**, *35*, 1381–1390. [CrossRef]
10. Smitt, S.; Tolstorebrov, I.; Gullo, P.; Pardiñas, A.; Hafner, A. Energy use and retrofitting potential of heat pumps in cold climate hotels. *J. Clean. Prod.* **2021**, *298*, 126799. [CrossRef]
11. Bolaji, B.; Huan, Z. Ozone depletion and global warming: Case for the use of natural refrigerant—A review. *Renew. Sustain. Energy Rev.* **2013**, *18*, 49–54. [CrossRef]
12. Frank, T. *Impact of Fluorinated Refrigerants and Their Degradation Products on the Environment and Health*; Technical Report; Refolution Industrielkälte GmbH: Karlsruhe, Germany, 2021.
13. Koronen, C.; Tedesco, R. *One Step Forward, Two Steps Back—A Deep Dive into the Climate Impact of Modern Fluorinated Refrigerants*; Technical Report; Environmental Coalition on Standards (ECOS): Brussels, Belgium, 2021.
14. Mota-Babiloni, A.; Makhnatch, P. Predictions of European refrigerants place on the market following F-gas regulation restrictions. *Int. J. Refrig.* **2021**, *127*, 101–110. [CrossRef]
15. Zolcer Skačanová, K.; Battesti, M. Global market and policy trends for CO_2 in refrigeration. *Int. J. Refrig.* **2019**, *107*, 98–104. [CrossRef]
16. Lorentzen, G. Revival of carbon dioxide as a refrigerant. *Int. J. Refrig.* **1994**, *17*, 292–301. [CrossRef]
17. Lorentzen, G.; Pettersen, J. A new, efficient and environmentally benign system for car air-conditioning. *Int. J. Refrig.* **1993**, *16*, 4–12. [CrossRef]
18. Nekså, P.; Rekstad, H.; Zakeri, G.; Schiefloe, P.A. CO_2-heat pump water heater: Characteristics, system design and experimental results. *Int. J. Refrig.* **1998**, *21*, 172–179. [CrossRef]
19. Nekså, P. CO_2 heat pump systems. *Int. J. Refrig.* **2002**, *25*, 421–427. [CrossRef]
20. Stene, J. Residential CO_2 heat pump system for combined space heating and hot water heating. *Int. J. Refrig.* **2005**, *28*, 1259–1265. [CrossRef]
21. Tosato, G.; Artuso, P.; Minetto, S.; Rossetti, A.; Allouche, Y.; Banasiak, K. Experimental and numerical investigation of a transcritical CO_2 air/water reversible heat pump: Analysis of domestic hot water production. In Proceedings of the 14th IIR-Gustav Lorentzen Conference on Natural Refrigerants, Kyoto, Japan, 6–9 December 2020; IIR: Paris, France, 2020.
22. Dai, B.; Qi, H.; Liu, S.; Zhong, Z.; Li, H.; Song, M.; Ma, M.; Sun, Z. Environmental and economical analyses of transcritical CO_2 heat pump combined with direct dedicated mechanical subcooling (DMS) for space heating in China. *Energy Convers. Manag.* **2019**, *198*, 111317. [CrossRef]
23. Byrne, P.; Miriel, J.; Lenat, Y. Design and simulation of a heat pump for simultaneous heating and cooling using HFC or CO_2 as a working fluid. *Int. J. Refrig.* **2009**, *32*, 1711–1723. [CrossRef]
24. Diaby, A.T.; Byrne, P.; Maré, T. Simulation of heat pumps for simultaneous heating and cooling using CO_2. *Int. J. Refrig.* **2019**, *106*, 616–627. [CrossRef]
25. Liu, Y.; Groll, E.A.; Yazawa, K.; Kurtulus, O. Theoretical analysis of energy-saving performance and economics of CO_2 and NH_3 heat pumps with simultaneous cooling and heating applications in food processing. *Int. J. Refrig.* **2016**, *65*, 129–141. [CrossRef]
26. Adriansyah, W. Combined air conditioning and tap water heating plant using CO_2 as refrigerant. *Energy Build.* **2004**, *36*, 690–695. [CrossRef]
27. Farsi, A.; Mohammadi, S.; Ameri, M. An efficient combination of transcritical CO_2 refrigeration and multi-effect desalination: Energy and economic analysis. *Energy Convers. Manag.* **2016**, *127*, 561–575. [CrossRef]

28. Singh, S.; Hafner, A.; Banasiak, K.; Seshadri, S.; Maiya, P.; Smitt, S.; Gabrielii, C.H. Heat pump/chiller system for centralized kitchens in India. In Proceedings of the 14th IIR-Gustav Lorentzen Conference on Natural Refrigerants, Kyoto, Japan, 7–9 December 2020; IIR: Paris, France, 2020.
29. Smitt, S.; Tolstorebrov, I.; Hafner, A. Integrated CO_2 system with HVAC and hot water for hotels: Field measurements and performance evaluation. *Int. J. Refrig.* **2020**, *116*, 59–69. [CrossRef]
30. Smitt, S.; Tolstorebrov, I.; Hafner, A. Performance improvement of integrated CO_2 systems with HVAC and hot water for hotels. *Therm. Sci. Eng. Prog.* **2021**, *23*, 100869. [CrossRef]
31. Tosato, G.; Girotto, S.; Minetto, S.; Rossetti, A.; Marinetti, S. An integrated CO_2 unit for heating, cooling and DHW installed in a hotel. Data from the field. *J. Phys. Conf. Ser.* **2020**, *1599*, 012058. [CrossRef]
32. Hafner, A.; Girotto, S.; Tosato, G. *CO_2 Heat Pump Water Chillers*; Eurammon Symposium/Webinar: Frankfurt, Germany, 2020.
33. Pardiñas, Á.Á.; Hafner, A.; Banasiak, K. Novel integrated CO_2 vapour compression racks for supermarkets. Thermodynamic analysis of possible system configurations and influence of operational conditions. *Appl. Therm. Eng.* **2018**, *131*, 1008–1025. [CrossRef]
34. Dassault Systems. DYMOLA Systems Engineering: Multi-Engineering Modeling and Simulation based on Modelica and FMI. 2019. Available online: https://www.3ds.com/products-services/catia/products/dymola/ (accessed on 1 May 2021).
35. TLK-Thermo GmbH. TIL Suite—Simulates Thermal Systems. 2020. Available online: https://www.tlk-thermo.com/index.php/en/software/til-suite (accessed on 1 May 2021).
36. TLK-Thermo GmbH. TILMedia Suite—Software Package for Calculating the Properties of Thermophysical Substances. 2020. Available online: https://www.tlk-thermo.com/index.php/en/software/tilmedia-suite (accessed on 1 May 2021).
37. Wagner, W. *Strömung und Druckverlust (Flow and Pressure Drop)*; Vogel: Höchberg, Germany, 2008; p. 67.
38. Haaf, S. Wärmeübertragung in luftkühlern (Heat transfer in air coolers). In *Wärmeaustauscher (Heat Exchangers)*; Springer: Berlin/Heidelberg, Germany, 1988; pp. 435–491.
39. Schmidt, T.E. Heat transfer calculations for extended surfaces. *Refrig. Eng.* **1949**, *57*, 351–357.
40. Huang, D.; Wu, Z.; Sunden, B. Pressure drop and convective heat transfer of Al2O3/water and MWCNT/water nanofluids in a chevron plate heat exchanger. *Int. J. Heat Mass Transf.* **2015**, *89*, 620–626. [CrossRef]
41. Gullo, P.; Elmegaard, B.; Cortella, G. Advanced exergy analysis of a R744 booster refrigeration system with parallel compression. *Energy* **2016**, *107*, 562–571. [CrossRef]
42. Brennen, C.E. *Fundamentals of Multiphase Flow*; Cambridge University Press: Cambridge, UK, 2005. [CrossRef]
43. Elbel, S.; Hrnjak, P. Experimental validation of a prototype ejector designed to reduce throttling losses encountered in transcritical R744 system operation. *Int. J. Refrig.* **2008**, *31*, 411–422. [CrossRef]
44. Gullo, P.; Hafner, A.; Banasiak, K. Transcritical R744 refrigeration systems for supermarket applications: Current status and future perspectives. *Int. J. Refrig.* **2018**, *93*, 269–310. [CrossRef]
45. Norwegian Standard (NS). NS-EN 14825:2018 (English Translation). *Air Conditioners, Liquid Chilling Packages and Heat Pumps, with Electrically Driven Compressors, for Space Heating and Cooling: Testing and Rating at Part Load Conditions and Calculation of Seasonal Performance*; Norwegian Council for Building Standardization: Oslo, Norway, 2018.
46. Meteotest AG. Meteonorm Software—Worldwide Irradiation Data. 2021. Available online: https://meteonorm.meteotest.ch/en/ (accessed on 1 May 2021).
47. United States Environmental Protection Agency. Refrigerant Transition & Environmental Impacts. 2020. Available online: https://www.epa.gov/mvac/refrigerant-transition-environmental-impacts (accessed on 23 June 2021).
48. EMERSON Climate Technologies. Refrigerant Choices for Commercial Refrigeration—Finding the Right Balance. Technical report No.: TGE124-091/E. 2010. Available online: https://climate.emerson.com/ (accessed on 18 June 2021).
49. European Environment Agency. Greenhouse Gas Emission Intensity of Electricity Generation. 2020. Available online: https://www.eea.europa.eu/data-and-maps/indicators/overview-of-the-electricity-production-3/assessment-1 (accessed on 23 June 2021).
50. Rezayan, O.; Behbahaninia, A. Thermoeconomic optimization and exergy analysis of CO_2/NH_3 cascade refrigeration systems. *Energy* **2011**, *36*, 888–895. [CrossRef]
51. Sanaye, S.; Shirazi, A. Thermo-economic optimization of an ice thermal energy storage system for air-conditioning applications. *Energy Build.* **2013**, *60*, 100–109. [CrossRef]
52. Gullo, P.; Elmegaard, B.; Cortella, G. Energetic, exergetic and exergoeconomic analysis of CO_2 refrigeration systems operating in hot climates. In Proceedings of the 28th International Conference on Efficiency, Cost, Optimization, Simulation and Environmental Impact of Energy Systems, Pau, France, 30 June–3 July 2015.
53. Fazelpour, F.; Morosuk, T. Exergoeconomic analysis of carbon dioxide transcritical refrigeration machines. *Int. J. Refrig.* **2014**, *38*, 128–139. [CrossRef]
54. Garrett, D.E. *Chemical Engineering Economics*; Springer Science & Business Media: Berlin/Heidelberg, Germany 2012.
55. Wang, Y.; Ye, Z.; Song, Y.; Yin, X.; Cao, F. Energy, exergy, economic and environmental analysis of refrigerant charge in air source transcritical carbon dioxide heat pump water heater. *Energy Convers. Manag.* **2020**, *223*, 113209. [CrossRef]
56. Blarke, M.B. Towards an intermittency-friendly energy system: Comparing electric boilers and heat pumps in distributed cogeneration. *Appl. Energy* **2012**, *91*, 349–365. [CrossRef]

57. Pardiñas, Á.Á.; Contiero, L.; Hafner, A.; Banasiak, K.; Larsen, L.F. Attaining a higher flexibility degree in CO_2 compressor racks. In Proceedings of the 14th IIR-Gustav Lorentzen Conference on Natural Refrigerants, Kyoto, Japan, 6–9 December 2020; IIR: Paris, France, 2020.
58. Eurostat. Electricity Prices for Non-Household Consumers. 2020. Available online: https://ec.europa.eu/eurostat/statistics-explained/index.php?title=Electricity_price_statistics (accessed on 1 June 202).